Journal of Visualized Experiments

Fabrication of Zero Mode Waveguides for High Concentration Single Molecule Microscopy

--Manuscript Draft--

Article Type:	Methods Article - JoVE Produced Video
Manuscript Number:	JoVE61154R1
Full Title:	Fabrication of Zero Mode Waveguides for High Concentration Single Molecule Microscopy
Section/Category:	JoVE Biochemistry
Keywords:	zero mode waveguides; nano-aperture; single molecule fluorescence; nanosphere lithography; colloidal crystal; self-assembly
Corresponding Author:	Kevin Y Chen University of Pennsylvania Perelman School of Medicine Philadelphia, Pennsylvania UNITED STATES
Corresponding Author's Institution:	University of Pennsylvania Perelman School of Medicine
Corresponding Author E-Mail:	chekevin@alumni.upenn.edu
Order of Authors:	Kevin Y. Chen
	Ryan M. Jamiolkowski
	Alyssa M. Tate
	Shane A. Fiorenza
	Shawn H. Pfeil
	Yale E. Goldman
Additional Information:	
Question	**Response**
Please indicate whether this article will be Standard Access or Open Access.	Standard Access (US$2,400)
Please indicate the **city, state/province, and country** where this article will be **filmed**. Please do not use abbreviations.	Philadelphia, PA, USA

TITLE:

Fabrication of Zero Mode Waveguides for High Concentration Single Molecule Microscopy

AUTHORS AND AFFILIATIONS:

Kevin Y. Chen[1], Ryan M. Jamiolkowski[1], Alyssa M. Tate[1], Shane A. Fiorenza[2], Shawn H. Pfeil[2], Yale E. Goldman[1]

[1]Pennsylvania Muscle Institute, Perelman School of Medicine, University of Pennsylvania, Philadelphia, PA, USA

[2]Department of Physics, West Chester University, West Chester, PA, USA

Corresponding Authors:

Shawn H. Pfeil (spfeil@wcupa.edu)

Yale E. Goldman (goldmany@upenn.edu)

Email Addresses of Co-Authors:

Kevin Y. Chen (chekevin@alumni.upenn.edu)

Ryan M. Jamiolkowski (jamiolk@gmail.com)

Alyssa M. Tate (amtate@udel.edu)

Shane A. Fiorenza (shane.fiorenza@colorado.edu)

KEYWORDS:

zero mode waveguides, nano-aperture, single molecule fluorescence, nanosphere lithography, colloidal crystal, self-assembly

SUMMARY:

Described here is a nanosphere lithography method for parallel fabrication of zero mode waveguides, which are arrays of nanoapertures in a metal-clad glass microscopy coverslip for single molecule imaging at nano- to micromolar concentrations of fluorophores. The method takes advantage of colloidal crystal self-assembly to create a waveguide template.

ABSTRACT:

In single molecule fluorescence enzymology, background fluorescence from labeled substrates in solution often limits fluorophore concentration to pico- to nanomolar ranges, several orders of magnitude less than many physiological ligand concentrations. Optical nanostructures called zero mode waveguides (ZMWs), which are 100−200 nm in diameter apertures fabricated in a thin conducting metal such as aluminum or gold, allow imaging of individual molecules at micromolar concentrations of fluorophores by confining visible light excitation to zeptoliter effective volumes. However, the need for expensive and specialized nanofabrication equipment has precluded the widespread use of ZMWs. Typically, nanostructures such as ZMWs are obtained by direct writing using electron beam lithography, which is sequential and slow. Here, colloidal, or nanosphere, lithography is used as an alternative strategy to create nanometer-scale masks for waveguide fabrication. This report describes the approach in detail, with practical considerations for each phase. The method allows thousands of aluminum or gold ZMWs to be

made in parallel, with final waveguide diameters and depths of 100−200 nm. Only common lab equipment and a thermal evaporator for metal deposition are required. By making ZMWs more accessible to the biochemical community, this method can facilitate the study of molecular processes at cellular concentrations and rates.

INTRODUCTION:

Single-molecule techniques such as single molecule fluorescence resonance energy transfer (smFRET) or single molecule fluorescence correlation spectroscopy (FCS) are powerful tools for molecular biophysics, allowing the study of dynamic movements, conformations, and interactions of individual biomolecules in processes such as transcription[1-3], translation[4-6], and many others[7]. For smFRET, total internal reflection fluorescence (TIRF) microscopy is a common method because many tethered molecules may be followed over time, and the evanescent wave generated by TIR is limited to a 100−200 nm region adjacent to the coverslip[8]. However, even with this restriction on excitation volume, fluorophores of interest still need to be diluted to pM or nM ranges in order to detect single molecule signals above background fluorecence[9]. Since the Michaelis-Menten constants of cellular enzymes are typically in the µM to mM range[10], biochemical reactions in single molecule studies are usually much slower than those in the cell. For example, protein synthesis occurs at 15−20 amino acids per second in *E. coli*[11,12], while most prokaryotic ribosomes in smFRET experiments translate at 0.1−1 amino acid per second[13]. In protein synthesis, crystal structures and smFRET on stalled ribosomes showed that transfer RNAs (tRNAs) fluctuate between 'hybrid' and 'classical' states before the tRNA-mRNA translocation step[14,15]. However, when physiological concentrations of the translocation GTPase factor, EF-G, was present, a different conformation, intermediate between the hybrid and classical states, was observed in smFRET[6]. Studying dynamic molecular processes at rates and concentrations similar to those in the cell is important, but remains a technical challenge.

A strategy to increase the fluorescent substrate concentration is the use of metal-based, sub-visible wavelength apertures, called zero mode waveguides (ZMWs), to generate confined excitation fields that selectively excite biomolecules localized within the apertures[16] (**Figure 1**). The apertures are typically 100−200 nm in diameter and 100−150 nm in depth[17]. Above a cutoff wavelength related to the size and shape of the wells ($\lambda_c \approx 2.3$ times the diameter for circular waveguides with water as the dielectric medium[18]), no propagating modes are allowed in the waveguide, hence the term zero mode waveguides. However, an oscillating electromagnetic field, termed an evanescent wave, exponentially decaying in intensity still tunnels a short distance into the waveguide[18,19]. Although similar to TIR evanescent waves, ZMW evanescent waves have a shorter decay constant, resulting in 10−30 nm effective excitation region within the waveguide. At micromolar concentrations of fluorescently labeled ligands, only one or a few molecules are simultaneously present within the excitation region. This restriction of the excitation volume and consequent reduction of background fluorescence enables fluorescence imaging of single molecules at biologically relevant concentrations. This has been applied to many systems[20], including FCS measurements of single protein diffusion[21], single molecule FRET measurements of low-affinity ligand-protein[22] and protein-protein interactions[23], and spectro-electrochemical measurements of single molecular turnover events[24].

ZMWs have been produced by directly patterning a metal layer using ion beam milling[25,26] or electron beam lithography (EBL) followed by plasma-etching[16,27]. These maskless lithography methods create waveguides in series and typically require access to specialized nanofabrication facilities, preventing widespread adoption of ZMW technology. Another method, ultraviolet nanoimprint lithography lift-off[28], uses a quartz slide mold to press an inverse ZMW template onto a resist film like a stamp. While this method is more streamlined, it still requires EBL for fabrication of the quartz mold. This article presents the protocol for a simple and inexpensive templated fabrication method that does not require EBL or ion-beam milling and is based on close-packing of nanospheres to form a lithographic mask.

Nanosphere or "natural" lithography, which was first proposed in 1982 by Deckman and Dunsmuir[29,30], uses the self-assembly of monodisperse colloidal particles, ranging from tens of nanometers to tens of micrometers[31], to create templates for surface patterning via etching and/or deposition of materials. The two-dimensional (2D) or three-dimensional (3D) extended periodic arrays of colloidal particles, referred to as colloidal crystals, are characterized by a bright iridescence from scattering and diffraction[32]. Although less widely used than electron-beam or photolithography, this masking methodology is simple, low cost, and easily scaled down to create feature sizes below 100 nm.

Directing the self-assembly of colloidal particles determines the success of using colloidal crystals as masks for surface patterning. If the size and shape of particles are homogeneous, colloidal particles can be readily self-assembled with hexagonal packing, driven by entropic depletion[33]. Water evaporation after drop-coating is an effective route to sediment the colloidal particles, although other methods include dip-coating[34], spin coating[35], electrophoretic deposition[36], and consolidation at an air-water interface[37]. The protocol presented below is based on the evaporation sedimentation method, which was the simplest to implement. The triangular interstices between close-packed polystyrene beads form openings in which to plate a sacrificial metal, forming posts (**Figure 2** and **Supplemental Figure 1**). Brief annealing of the beads before this step adjusts the shape and diameter of these posts. The beads are removed, a final metal layer is deposited around the posts, and then the posts are removed. After the two metal deposition steps onto the colloidal nanomask, removal of the intermediate posts, and surface chemistry modification for passivation and tethering, ZMW arrays are ready to use for single molecule imaging. More extensive characterization of the ZMW optical properties after fabrication can found in an accompanying article[38]. Besides a thermal evaporator for vapor deposition of the metals, no specialized tools are required.

PROTOCOL:

NOTE: All steps can be completed in general lab space.

1. Glass coverslip cleaning

1.1. To provide a clean surface for evaporative deposition of colloidal particles, place 24 x 30 mm optical borosilicate glass coverslips (0.16–0.19 mm thickness) within the grooved inserts of a coplin glass staining jar for cleaning.

NOTE: Make sure the coverslips stand upright and are well-separated so that all surfaces are clearly exposed during the cleaning process.

1.2. Pour enough acetone in the staining jar to cover the coverslips, place the cover on, and sonicate for 10 min at 40 °C.

1.3. Pour out the acetone and rinse the coverslips by filling the staining jar with distilled H_2O and pouring out the water. Repeat 2 more times.

1.4. Repeat the acetone sonication (steps 1.2 and 1.3) once more.

1.5. Pour enough 200 mM KOH in the jar to cover the coverslips and sonicate, covered, for 20 min at 40 °C.

NOTE: The KOH slightly etches the glass.

1.6. Rinse the coverslips with distilled H_2O 6 times.

1.7. Add ethanol to cover the coverslips, add the lid, and sonicate for 10 min at 40 °C.

1.8. Rinse the coverslips with distilled H_2O 3 times.

1.9. Pick up each coverslip at the edge using gentle forceps and dry the coverslips with N_2 gas. Touch only the edges of the coverslip. Place each of the dried, cleaned coverslips in an individual clean Petri dish.

2. Evaporative deposition of polystyrene beads

2.1. To create the colloidal crystal mask for the ZMW array, centrifuge 50 µL of 1 µm diameter, non-functionalized polystyrene beads (2.5% w/v in water) at 15,000 x *g*, 25 °C for 5 min.

NOTE: Before pipetting the beads, the stock solution should be briefly vortexed in case the beads have settled to the bottom of the bottle.

2.2. Discard the supernatant, leaving as little water remaining as possible.

NOTE: Residual water can change the evaporation properties of the ethanol resuspension[39], so removal of a small amount of beads in order to remove all of the water is acceptable.

2.3. Resuspend the beads from step 2.2 in 50 µL of 1:400 TritonX-100:ethanol solvent. Pipette up and down several times to thoroughly mix the beads with the solvent.

NOTE: TritonX-100:ethanol solvent should be sealed with paraffin film after use and prepared fresh once a month. The beads tend to adhere to the sides of a plastic vessel, such as a microcentrifuge tube, so pipette along the sides to ensure that all beads are resuspended.

2.4. To set up a humidity chamber for deposition, place 6 Petri dishes, each with one coverslip, on a bench in a line with lids left slightly ajar. In each dish, move the coverslip to the open region so that the coverslips are exposed to the environment when the humidity is increased in the next step.

2.5. Place a hygrometer and a small electric fan centered behind the Petri dishes.

2.6. Record the starting relative humidity (RH) in the lab. Fill a 200 mL beaker with 150–200 mL of ~75 °C water and place it behind the fan.

2.7. Turn on the fan and cover the Petri dishes, fan, beaker, and hygrometer with an overturned, transparent plastic storage container (66 cm x 46 cm x 38 cm).

2.8. Let the RH in the chamber rise to 70–75%, which typically takes 5–10 min.

NOTE: If the ambient lab RH is low (below ~50%), let the chamber reach a higher RH, but no higher than 80%, to compensate for loss of humidity during deposition (see below).

2.9. When the RH reaches 70–75%, record the RH and lift up the plastic storage container slightly to quickly place covers on the Petri dishes, which prevents over-wetting of the coverslips.

NOTE: The temperature in the chamber will be slightly warmer than room temperature, typically 25–26 °C, as a result of humidification. If moisture is visible on the coverslips, then the glass surfaces are too wet. A commercial glove box might simplify this part of the protocol.

2.10. Let the RH in the chamber continue to rise to 85%. At that point, record the RH in the humidity chamber and pipette 5 µL of the bead suspension onto the center of each coverslip.

2.11. Close the chamber and Petri dishes after each deposition to minimize loss of humidity. Aim to finish all 6 depositions within 2 min.

2.12. Record the RH in the chamber after the deposition.

NOTE: The RH after deposition will help gauge how fast humidity was lost during deposition, which depends on ambient lab conditions. For a typical successful run, the chamber will start at 85% RH prior to deposition and end at 70–75% RH after the deposition.

2.13. Let the bead droplets spread and dry for 5 min.

NOTE: If the colloidal crystals have many holes or multilayered regions, then the chamber was likely too humid or dry, respectively. Adjust the relative humidity at which to close the Petri dishes and begin the depositions (see the results section for further discussion of optimization).

3. Bead annealing for reducing pore size in the colloidal crystal template

3.1. To provide a uniform temperature surface for annealing of the polystyrene beads, which narrows the inter-bead interstices and rounds the interstices' corners, place a flat, milled aluminum plate on top of a standard ceramic hot plate.

3.2. Set the temperature of the hot plate to 107 °C, the glass transition temperature of polystyrene[40].

NOTE: To obtain stable and accurate temperature, a thermocouple probe was held in a 2−3 mm wide and 4−5 mm deep hole in the aluminum plate.

3.3. Place a coverslip containing the bead template on the hot aluminum plate and anneal for 20 s (see the discussion section for explanation of melting time).

3.4. After heating, remove the coverslip from the aluminum plate and promptly place it on another room temperature aluminum surface to cool it.

NOTE: It is helpful to either have the coverslips hang slightly over the edge of the plate or mill shallow channels (see the accompanying video) into the plate to facilitate pickup of the coverslips. The protocol can be interrupted here, but bead templates should be stored in covered, clean Petri dishes in a cool, dry environment to preserve the polystyrene templates.

4. Nanofabrication of aluminum zero mode waveguides using the colloidal crystal template

4.1. Using thermal or electron-beam evaporative deposition, deposit 300 nm of copper at 2 Å/s over the colloidal crystal template to generate posts in the interstices between the beads.

4.2. Remove excess metal on top of the beads by gently pressing the surface with tape. Slowly peel the tape to pull off the metal.

NOTE: Some small patches of reflective excess metal may remain after the tape pull, and these can often be removed by a stream of N_2 gas. If substantial patches of reflective excess metal remain after the tape pull, try soaking the templates in toluene for 2 h to partially dissolve the polystyrene beads. Wash the coverslips with distilled water, dry with N_2, and repeat the tape pull. The additional soak should not completely dissolve the beads, as the beads help protect the posts from damage during the tape pull.

4.3. To dissolve the polystyrene beads, place the bead templates in toluene and soak overnight.

CAUTION: Toluene fumes may be toxic. Work with toluene under a well-ventilated hood and wear personal protective equipment, including gloves, safety glasses, and a lab coat. Toluene should be stored in ventilated cabinets designated for flammable liquids.

4.4. After the toluene incubation, rinse the templates once with chloroform and twice with ethanol. Handle coverslips carefully at this point because the delicate 200–300 nm tall metal posts are now exposed. Dry the templates with N_2 and remove residual polymer and contaminants in an oxygen plasma cleaner for 30 min.

CAUTION: Chloroform fumes may be toxic. Work with chloroform under a well-ventilated hood and wear personal protective equipment, including gloves, safety glasses, and a lab coat. Chloroform should be stored in ventilated cabinets away from other flammable solvents.

4.5. Using thermal or electron-beam evaporative deposition, deposit 3 nm of a titanium adhesion layer at 1 Å/s followed by 100–150 nm of aluminum at 4 Å/s around and on top of the copper posts.

NOTE: One can use thicker cladding to obtain deeper guides and better attenuation of background fluorescence, but this also decreases the yield after exposing and dissolving the posts in the next step (see the discussion section).

4.6. To dissolve the metal posts, soak the coverslips in copper etchant (citric acid-based; **Table of Materials**) for 2 h.

CAUTION: Metal etchant can cause skin burns. Work with etchants under a well-ventilated hood and wear protective equipment. Wash hands thoroughly after handling. Metal etchant should be stored in ventilated cabinets designated for corrosive liquids.

4.7. Rinse the coverslips with distilled water, dry with N_2, and gently buff the surface of the metal cladding with lens paper to expose any posts that are still covered in cladding. Place the coverslips back in copper etchant for another 2 h, then rinse again with distilled water and dry with N_2.

NOTE: ZMW slides should be stored in covered, clean Petri dishes to keep them free of contaminants.

5. Nanofabrication of gold zero mode waveguides using the colloidal crystal template

NOTE: The method to fabricate gold ZMWs (**Supplemental Figure 1**), which mirrors the protocol to fabricate aluminum ZMWs, is provided in this section.

5.1. Using thermal or electron beam evaporative deposition, deposit 3 nm of a titanium adhesion layer at 1 Å/s followed by 300 nm of aluminum at 4 Å/s.

5.2. Remove excess metal on top of the beads by gently pressing the surface with tape. Slowly peel the tape to pull off the metal.

5.3. To dissolve the polystyrene beads, place the bead templates in toluene and soak overnight.

5.4. After the toluene incubation, rinse the templates once with chloroform and twice with ethanol. Dry the templates with N_2 and remove residual polymer contaminants in an oxygen plasma cleaner for 30 min.

5.5. Using thermal or electron beam evaporative deposition, deposit 100−150 nm of gold at 5 Å/s around and on top of the aluminum posts.

5.6. To dissolve the metal posts, soak the coverslips in aluminum etchant (phosphoric acid-based; **Table of Materials**) for 1 h.

5.7. Rinse the coverslips with distilled water, dry with N_2, and gently buff the surface of the metal cladding with lens paper to expose any posts that are still covered in cladding. Place the coverslips back in aluminum etchant for 1 h, then rinse again with distilled water and dry with N_2.

NOTE: ZMW slides should be stored in covered, clean Petri dishes.

REPRESENTATIVE RESULTS:

The self-assembly of the polystyrene colloidal particles via evaporative sedimentation (steps 2.1−2.13) can produce a range of results since it requires control of the solvent evaporation rate. However, because the depositions are fast (10−15 min per round), the procedure can be quickly optimized for different ambient lab conditions. **Figure 3A** shows a well-formed colloidal template after deposition and evaporation. Macroscopically, the region of beads is circular, with borders defined by an opaque, multilayered ring of beads. The translucent, but not white regions in the image are the desired monolayer areas. **Figure 3B** shows a colloidal template that was packed in an overly humid environment (80% RH when Petri dishes were closed). These templates tend not to have a clean circular boundary and have multilayered tendrils extending outward. The deposition is acceptable and can be used in subsequent phases, but the holes in the lattice reduce the number of useable ZMW array areas for single molecule imaging. **Figure 3C** shows a colloidal template that was packed in an overly dry environment (65% RH when Petri dishes were closed). These templates are usually smaller in diameter compared to the ideal, well spread templates. The deposition can be used, but the multilayered, white regions, which streak inward, reduce the area usable for imaging. Thus, we do not recommend performing more than 6 depositions at a time since depositions toward the end of the process will occur at a lower humidity as the chamber is opened and closed. **Figure 3D** shows the rainbow pattern produced by diffraction of reflected light from the polystyrene crystal. This pattern can be used to confirm success and quality of crystal packing by eye. **Figure 3E,F** shows atomic force microscopy (AFM) images of well-packed colloidal templates. The defects between grains arise from jamming during the evaporative sedimentation[41], and distinct grains can be seen with a 10x objective. Thus,

examining the colloid depositions with a low-power light microscope can also be used to assess packing.

After deposition of copper onto the annealed colloidal templates (step 4.1), the rainbow diffraction pattern should still be visible and enhanced by the reflective metal coating the tops of the beads (**Figure 4A,B**). The templates lose the reflective rainbow diffraction pattern after the Scotch tape pull (step 4.2) that removes excess copper (**Figure 4C**). **Figure 4D,E** shows AFM images of a typical field of copper posts after metal deposition. The defects in between the colloidal crystal grains in **Figure 3E** are visible in the copper post images as larger regions of copper. Analysis of AFM images shows that, for a copper deposition thickness of 300 nm, the eventual copper posts average 255 nm (**Figure 4F**) in height and 121 nm in diameter (**Figure 4G**).

Deposition of the aluminum cladding (step 4.5) where the beads were and on top of the copper posts, and subsequent dissolution of the posts (steps 4.6 and 4.7) result in the aluminum ZMWs shown in **Figure 5A–C**. Defects between the colloidal crystal grains are visible as larger openings (**Figure 5B**). The average distance between the ZMW centers in **Figure 5C** is 559 nm, consistent with the spacing set by the hexagonal close packing geometry of the 1 µm beads ($\frac{2}{\sqrt{3}} * 500\ \mathrm{nm} = 557\ \mathrm{nm}$). Using polystyrene templates that were annealed for 20 s results in waveguides that are on average 118 nm in diameter (**Figure 5D,E**), consistent with the post diameters and sufficiently small to cut off propagation of visible light. A height profile of a waveguide from **Figure 5D** also shows that it is ~120 nm deep.

Single molecule FRET was performed in the ZMWs to test for functionality (**Figure 6A**). A typical field of ZMWs for imaging is shown in **Figure 6B**, which contains >3000 waveguides in a 40 x 80 µm field of view. The ZMWs were first passivated using protocols described previously[42,43]. Briefly, the aluminum ZMWs were passivated with poly(vinylphosphonic acid) to coat the aluminum cladding followed by methoxy-terminated polyethylene glycol (PEG) doped with biotin-terminated PEG to coat the glass bottoms of the ZMWs. Gold ZMWs can be passivated with thiol-derivatized PEG to coat the gold cladding followed by a similar PEG treatment for the glass bottoms. Flow chambers, ~20 µL volume, were then constructed for single molecule imaging[44]. Single molecule FRET imaging of the DNA duplexes was performed as described previously[38]. Briefly, 100 pM−1 nM of cyanine-3/cyanine-5 (Cy3/Cy5), biotinylated DNA duplexes (33 base pair length) were incubated for 10 min in flow channels functionalized with streptavidin (5 min incubation, 0.5 mg/mL solution). The concentration of labeled macromolecules can be titrated to achieve ~20% loading of the waveguides with one molecule, leading to <5% waveguides loaded with more than one molecule, based on Poisson distributed loading (most waveguides, ~75%, will have no molecules)[45]. Unbound DNA was washed away with nuclease-free duplex buffer followed by illumination buffer (0.3% [w/v] glucose, 300 µg/mL glucose oxidase, 120 µg/mL catalase, and 1.5 mM Trolox [6-hydroxy-2,5,7,8-tetramethyl-chromane-2-carboxylic acid]). Non-biotinylated Cy5-labeled DNA duplexes (33 base pair length) were present in the illumination buffer at 0, 50, 100, and 500 nM as background fluorophores in solution. Single molecule FRET traces from the immobilized Cy3/Cy5 duplex DNA molecules were recorded with a custom-built TIRF microscope adjusted to epi-fluorescence conditions. Movies were recorded

with a 1.48 numerical aperture (NA) 100x oil immersion objective with alternating 532 nm and 640 nm excitation (100 ms exposure) and a dual view spectral splitter to record Cy3 and Cy5 emission simultaneously on an electron-multiplying charge-coupled device (EMCCD) camera. Single molecule FRET traces with single step bleaches in the Cy5 channel were detectable at all concentrations of ambient Cy5 tested (**Figure 6C–F**). In comparison, single molecules would only be detectable in TIRF illumination with pM to low nM solution fluorophore concentrations[46].

FIGURE LEGENDS:

Figure 1: Schematic of zero mode waveguides. Diagram of ZMW array with expanded cross-sectional diagram of a single ZMW on the right. Single fluorescently tagged enzymes of interest (brown ribosome with red circle to represent fluorescent dye) chemically immobilized (via the mRNA in this example) to the glass bottom of the ZMWs (typically functionalized with biotinylated-PEG) can be imaged with a typical laser-based epifluorescence microscopy setup. The 532 nm excitation light (green arrows) is reflected at the glass-metal boundary due to the small size of the aperture (100−200 nm diameter), but a non-propagating evanescent wave that decays exponentially in intensity is present within the ZMW. This results in a 10−30 nm effective illumination depth (green shading in aperture). Individual fluorescent ligands (blue tRNAs with green circles as fluorescent tags) at nM to μM concentrations are added. An individual ligand that diffuses into the aperture and interacts with the enzyme is imaged without prohibitive background fluorescence.

Figure 2: Schematic of colloidal templating method developed to fabricate aluminum ZMW arrays. Polystyrene beads, 1 μm in diameter, are deposited and self-assembled on a cleaned glass coverslip, as described in section 2 of the protocol. Beads are then annealed to reduce pore sizes (section 3), followed by copper deposition and bead dissolution in toluene. Aluminum is deposited around and on top of the copper posts, which are then selectively etched away to leave behind a hexagonal array of nanoapertures (section 4). For the last three steps, cross-sectional views are provided to the right of the plan views to show the widths and heights of the copper posts and aluminum ZMWs.

Figure 3: Representative results from evaporative deposition of colloids. **(A)** Example of optimal colloid deposition. **(B)** Example of an acceptable colloid deposition in which conditions were more humid (80% RH) than ideal. Holes in the crystal monolayer are apparent. **(C)** Example of an acceptable colloid deposition in which conditions were drier (65% RH) than optimal. The monolayer regions are slightly translucent while multilayered areas are white and opaque (perimeter and streaks inward). **(D)** A colloidal crystal illuminated with white light to highlight the rainbow diffraction from the crystals. **(E)** AFM image (tapping probe AFM in air) of a monolayer of hexagonally packed polystyrene beads from a successful colloid deposition (scale bar = 10 μm). (**F)** Expanded AFM image of packed beads (scale bar = 2 μm).

Figure 4: Macroscopic and microscopic images of ZMW templates after copper deposition. (A) Picture of slides after physical evaporation of copper on top of the bead templates. **(B)** Rainbow diffraction pattern from bead templates after copper deposition. **(C)** Picture of a template (right) after a tape pull to remove excess copper and the tape (left). **(D)** AFM image of copper posts after

tape pull and complete dissolution of the polystyrene beads (scale bar = 5 µm). **(E)** Higher magnification AFM image of panel D (scale bar = 2 µm). (**F)** Histogram of the copper post heights (defined as maximum height measurement within each post), n = 534. (**G)** Histogram of the copper post Feret diameters, n = 201. Feret diameter is the maximum distance between two parallel lines tangent to the post boundary (quantified in ImageJ[47]). To identify particles for analysis, a threshold halfway between the top of the cladding and the bottom glass surface was used.

Figure 5: Macroscopic and microscopic images of aluminum ZMWs. (A) Picture of slides after physical evaporative deposition of 150 nm of aluminum around and on top of the copper posts. **(B)** AFM image of aluminum ZMWs after post dissolution (scale bar = 5 µm). **(C)** Higher magnification image of panel B (scale bar = 0.2 µm). **(D)** Typical depth profile of an individual ZMW from panel C. Profile taken from the green line drawn in panel C. **(E)** Histogram of ZMW Feret diameters, n = 240. Feret diameters were measured as in **Figure 4**.

Figure 6: Single molecule FRET imaging in ZMWs. (A) Schematic (not to scale) of single molecule FRET imaging of Cy3, Cy5-labeled DNA duplexes in ZMWs with Cy5 labeled duplexes in the background. **(B)** Example field of ZMWs under white light illumination (scale bar = 10 µm). (**C–F)** Single molecule FRET recordings of DNA duplexes immobilized in the ZMWs in the presence of 0 **(C)**, 50 **(D)**, 100 **(E)**, and 500 nM **(F)** Cy5-labeled duplexes in solution. For each concentration, the top panel shows the Cy3 (green) and Cy5 (red) fluorescence intensity under 532 nm laser illumination (FRET imaging), middle panel shows the Cy5 fluorescence intensity under 640 nm laser illumination (direct acceptor excitation), and the lowest panel shows the FRET efficiency ($E_{apparent} = \frac{I_A}{I_A+I_D}$) calculated from the raw Cy3 (I_D) and Cy5 (I_A) fluorescence intensities. During imaging, the excitation wavelength alternated between 532 and 640 nm every 100 ms.

Supplemental Figure 1: Schematic of colloidal templating method developed to fabricate gold ZMW array. Protocol to fabricate gold ZMW array is analogous to protocol to fabricate aluminum ZMW array (**Figure 2**). Instead of depositing copper on top of the polystyrene beads, aluminum is deposited. After dissolving the beads in toluene, gold is deposited instead of aluminum on top of the posts. Aluminum posts are then selectively etched to leave behind gold ZMW array. For the last three steps, cross-sectional views are provided to the right of the plan views to show the widths and heights of the aluminum posts and gold ZMWs.

Supplemental Figure 2: Finite element modeling of electromagnetic field propagation in ZMWs. (**A–D)** Cross sections of the magnitude of the time-averaged Poynting vector (W/m^2) through a waveguide made from an unannealed template **(A,C)** and an annealed template **(B,D)**. Linearly polarized electromagnetic plane waves (1 W distributed over the area of the slide) at the wavelengths listed in the figure (400 nm or 1,000 nm) were projected onto the bottom surface, and the lowest (fundamental) mode, which has the lowest wavenumber, was computed using modeling software (**Table of Materials**) with the finite element method for solving Maxwell's equations and appropriate boundary conditions. The boundaries of the waveguides were assumed to be perfect electrical conductors, which is well approximated by aluminum or gold

walls. The cross-section from the unannealed waveguide template was determined by the hexagonal packing of 1 μm diameter circles, and the three-pointed tips from the resulting triangular shape were clipped to ~60 nm width to model a realistic physical aperture. The cross-section from the annealed templates was approximated as a circle 130 nm in diameter. Both waveguides had a 130 nm depth, similar to the cladding depth after fabrication. (**E,F)** In addition to excitation wavelengths of 400 nm and 1,000 nm, the models were solved at 100 excitation wavelengths evenly spaced between 400 nm and 1,000 nm, and the effective mode index (defined as $\frac{k_z}{k}$, where k_z is the wavenumber in the waveguide, which is decreased due to restriction in the transverse plane, and k is the excitation light wavenumber in vacuum) was plotted against excitation wavelength for the triangular **(E)** and circular **(F)** waveguides. For shorter wavelengths, higher modes are excited, and the effective mode index increases (max effective mode index is 1, which is the limiting case where the electromagnetic plane wave travels unbounded in the transverse dimension). The effective cutoff wavelengths of the waveguides were estimated as the wavelength at which the effective mode index drops to 0. Note that the circular guide $\lambda_{cutoff} = 221\ nm$ from finite element modelling **(F)** is consistent with the theoretical prediction of a circular waveguide's cutoff wavelength ($\lambda_{cutoff,analytical} = 1.7d = 221\ nm$, where d is the waveguide diameter).

Supplemental Figure 3: Representative results from Au ZMW fabrication. (A) Macroscopic picture of gold ZMW arrays. (**B–D)** AFM images of aluminum posts from a bead template that was not annealed **(B)**, a template that was annealed at 107 °C for 20 s **(C)**, and a template that was annealed at 107 °C for 25 s **(D)**. **(E)** AFM image of gold ZMWs after dissolution of aluminum posts. (**F)** Higher magnification AFM image of panel E. (**G)** Typical depth profile of a gold ZMW. Profile taken from the green line drawn in panel F (scale bar = 1 μm in **B**, **C**, **D**, and **F**; 5 μm in **E**).

DISCUSSION:

For the colloidal self-assembly (protocol section 2), the use of ethanol rather than water as the suspension solvent speeds the evaporation process so that templates are ready in 2−3 min after deposition rather than 1−2 h as in previous methods[48,49]. The evaporative sedimentation protocol presented here is also simpler than previous sedimentation protocols that require controlling surface tilt, temperature, and air volume above the suspension[49-51]. The particle volume fraction used in this protocol is 2.4%, higher than the 0.2−0.5% used in previous sedimentation methods[48], which resuspended colloids in water-glycerol mixtures for much longer settling time-scales. However, the quality of the depositions is robust to changes in the particle volume fraction, with past studies finding that it can be varied between 2−10%[49-51]. The grain sizes of the colloidal crystals obtained in a successful deposition from this protocol are 20−30 μm across, larger than grains from previous sedimentation methods (typically several hundred nanometers across)[48,49]. Macroscopically, the roughly 2 cm in diameter areas of colloidal monolayer are also comparable to the 1 cm areas produced by previous methods[49]. The large size of the colloidal crystal templates produced in this method also allows 3−5 separated flow chambers[44], each about 3−4 mm wide, to be made on each ZMW slide. Thus, multiple independent single molecule experiments can be performed on each slide.

Annealing the colloidal bead templates (protocol section 3) after self-assembly is a simple, but crucial step for sufficiently reducing background fluorescence with the ZMWs. As **Supplemental Figure 2** shows, the effective cutoff wavelength for a waveguide with the triangular cross-section from an unannealed template is 894 nm. In comparison, the effective cutoff wavelength for a 130 nm diameter circular waveguide from an annealed template is 221 nm, as determined both analytically (1.7 times the diameter of the guide[18]) and numerically. Using smaller beads for deposition could also reduce the size of the template pores, but the waveguides would then be spaced closer than 200 nm, which is around the diffraction limit of visible light. Furthermore, the waveguides would remain triangular in cross-section, which leads to nonsymmetric power propagation through the waveguide (**Supplemental Figure 2A–D**). One drawback of the annealing step is that variability in melting time can introduce fluctuations in waveguide diameter, so accurate timing helps to minimize variation between batches. The interstices start to close at annealing times longer than 25 s, and post diameters do not decrease very much between 20−25 s (**Supplemental Figure 3B–D**). A quick test for interstice closure is to check whether annealed templates still produce a rainbow diffraction pattern when illuminated with light and viewed at an angle. If not, the majority of interstices likely have closed. The relationship between annealing time and typical pore diameters has been presented earlier[38].

After achieving the desired pore size during the annealing step, copper is deposited (step 4.1) onto the templates to create a shadow of the mask. It is important to use line of sight deposition, with the metal approaching the template as perpendicularly as possible. Thus, increasing the distance between the sample and metal source as well as ensuring the plate holding the templates is not spinning, as is automatically done in some vapor deposition machines, will aid in minimizing lateral deposition of metal onto the polystyrene substrate. However, some lateral deposition is inevitable, which reduces the size of the interstitial hole and thus the post cross-section as more metal is deposited[52]. This results in pyramidal metal posts rather than prism-like structures[52].

Because the copper posts are likely pyramidal rather than prism shaped, aluminum deposition (step 4.5) on top of the posts also covers some of the sloped sides, blocking accessibility of the copper etchant for some of the posts. Thus, the lens paper buffing step (step 4.7 or 5.7) was added after the first soak in etchant to mechanically disrupt any copper posts still covered in aluminum. Depositing more copper to create taller posts also makes the posts more susceptible to mechanical disruption during the lens paper buffing. However, more than 500 nm of copper should not be deposited since the goal of deposition is to project the interstitial hole at the 500 nm midline of the 1 μm beads.

Another potential difficulty is the unintended removal of aluminum cladding during the lens paper buffing (step 4.7 or 5.7). It was found that loss of aluminum cladding during buffing became more frequent after the annealing step was added, likely due to increased polystyrene residue, which can interfere with aluminum adherence to glass (protocol section 3). However, the overnight toluene soak (step 4.3 or 5.3) after the tape pull resolved this issue. In the AFM image in **Figure 4E**, some residual rings of polystyrene can be seen between the posts, but the aluminum cladding still resisted multiple buffs in step 4.7. If loss of the aluminum cladding remains an issue

after the overnight toluene soak, an RCA-1 (standard clean-1) wash, piranha wash, or further oxygen plasma cleaning can be added to step 4.4 or 5.4. These wash steps can also be added after the final etch step (step 4.7 or 5.7) and before passivation in order to further clean the ZMWs.

The performance of the ZMWs in single molecule FRET experiments was similar to that of ZMWs fabricated with EBL. In a previous study[53] performing single molecule FRET on Cy3 labeled single stranded DNA with Cy5 labeled DNA helicase loader protein in solution (the same donor-acceptor arrangement as that in **Figure 6A**), FRET events were clearly discernible at 100 nM Cy5 background, were less clear (lower acceptor trace signal to noise) at 1 µM, and not discernible at 10 µM. We note that a previous study with commercial ZMWs reported single molecule FRET acceptor signals at background concentrations as high as 1 mM[54], higher than we and other previous studies[42,53] with in-house fabricated ZMWs have achieved. Further discussion of the signal-to-background performance among ZMWs is given in Jamiolkowski et al.[38]. Nonspecific interaction of fluorescent sample with the ZMW surfaces[53] is a common challenge limiting access to higher concentrations, especially if the diffusing fluorescent species in solution is a large macromolecule. Studies with ZMWs on complex biochemical systems such as translation have typically limited free fluorescent substrate concentrations to 100−250 nM[55-58]. Regardless of the intended application of the ZMWs, optimization of passivation methods for different systems will likely be necessary to maintain acceptable signal to noise at high concentrations.

Overall, the method presented here requires no specialized skills or equipment, allows parallel fabrication of many templates at once, and can be adapted to fabricate ZMWs in different metals. In this work, copper and aluminum were substituted with aluminum and gold, respectively, to fabricate gold ZMWs (**Supplemental Figure 3**). This is advantageous for labs that use passivation methods of gold rather than aluminum. In addition, gold ZMWs have been shown to enhance emission for fluorophores that absorb in the red region of the visible spectrum, while aluminum ZMWs enhance emission for fluorophores that absorb in the green region[59]. In the future, fluorescent signal intensity from ZMWs fabricated with this method might be enhanced by etching into the glass below the ZMW metal cladding using HF[16,26,60]. This brings the immobilized biomolecules farther away from the metal walls, which can quench fluorophores[61]. Furthermore, there is a maximum in excitation illumination intensity below the entrance of the aperture, and this has been exploited previously to enhance single molecule emission[26,60].

ACKNOWLEDGMENTS:

This work was supported by NIH grants R01GM080376, R35GM118139, and NSF Center for Engineering MechanoBiology CMMI: 15-48571 to Y.E.G., and by an NIAID pre-doctoral NRSA fellowship F30AI114187 to R.M.J.

DISCLOSURES:

The authors have nothing to disclose.

REFERENCES:

1. Kapanidis, A. N. et al. Initial transcription by RNA polymerase proceeds through a DNA-

611 scrunching mechanism. *Science.* **314** (5802), 1144-1147 (2006).
612 2. Santoso, Y. et al. Conformational transitions in DNA polymerase I revealed by single-molecule
613 FRET. *Proceedings of the National Academy of Sciences of the United States of America.* **107** (2),
614 715-720 (2010).
615 3. Herbert, K. M., Greenleaf, W. J., Block, S. M. Single-molecule studies of RNA polymerase:
616 motoring along. *Annual Review of Biochemistry.* **77**, 149-176 (2008).
617 4. Chen, C. et al. Dynamics of translation by single ribosomes through mRNA secondary
618 structures. *Nature Structural & Molecular Biology.* **20** (5), 582-588 (2013).
619 5. Chen, C. et al. Single-molecule fluorescence measurements of ribosomal translocation
620 dynamics. *Molecular Cell.* **42** (3), 367-377 (2011).
621 6. Jamiolkowski, R. M., Chen, C., Cooperman, B. S., Goldman, Y. E. tRNA Fluctuations Observed
622 on Stalled Ribosomes Are Suppressed during Ongoing Protein Synthesis. *Biophysical Journal.* **113**
623 (11), 2326-2335 (2017).
624 7. Myong, S., Stevens, B. C., Ha, T. Bridging Conformational Dynamics and Function Using Single-
625 Molecule Spectroscopy. *Structure.* **14** (4), 633-643 (2006).
626 8. Martin-Fernandez, M. L., Tynan, C. J., Webb, S. E. A 'pocket guide' to total internal reflection
627 fluorescence. *Journal of Microscopy.* **252** (1), 16-22 (2013).
628 9. Holzmeister, P., Acuna, G. P., Grohmann, D., Tinnefeld, P. Breaking the concentration limit of
629 optical single-molecule detection. *Chemical Society Reviews.* **43** (4), 1014-1028 (2014).
630 10. Scheer, M. et al. BRENDA, the enzyme information system in 2011. *Nucleic Acids Research.*
631 **39** (Database issue), D670-676 (2011).
632 11. Kudva, R. et al. Protein translocation across the inner membrane of Gram-negative bacteria:
633 the Sec and Tat dependent protein transport pathways. *Research in Microbiology.* **164** (6), 505-
634 534 (2013).
635 12. Talkad, V., Schneider, E., Kennell, D. Evidence for variable rates of ribosome movement in
636 Escherichia coli. *Journal of Molecular Biology.* **104** (1), 299-303 (1976).
637 13. Blanchard, S. C., Kim, H. D., Gonzalez, R. L., Jr., Puglisi, J. D., Chu, S. tRNA dynamics on the
638 ribosome during translation. *Proceedings of the National Academy of Sciences of the United*
639 *States of America.* **101** (35), 12893-12898 (2004).
640 14. Dunkle, J. A. et al. Structures of the bacterial ribosome in classical and hybrid states of tRNA
641 binding. *Science.* **332** (6032), 981-984 (2011).
642 15. Kim, H. D., Puglisi, J. D., Chu, S. Fluctuations of transfer RNAs between classical and hybrid
643 states. *Biophysical Journal.* **93** (10), 3575-3582 (2007).
644 16. Levene, M. J. et al. Zero-mode waveguides for single-molecule analysis at high
645 concentrations. *Science.* **299** (5607), 682-686 (2003).
646 17. Zhu, P., Craighead, H. G. Zero-mode waveguides for single-molecule analysis. *Annual Review*
647 *of Biophysics.* **41**, 269-293 (2012).
648 18. Pollack, G. L., Stump, D. R. *Electromagnetism*. Addison-Wesley. Boston, MA (2002).
649 19. Jackson, J. D. *Classical electrodynamics*. Third edition. Wiley. New York, NY (1999).
650 20. Crouch, G. M., Han, D., Bohn, P. W. Zero-mode waveguide nanophotonic structures for single
651 molecule characterization. *Journal of Physics D: Applied Physics.* **51** (19), 193001 (2018).
652 21. Wenger, J. et al. Dual-color fluorescence cross-correlation spectroscopy in a single
653 nanoaperture: towards rapid multicomponent screening at high concentrations. *Optics Express.*
654 **14** (25), 12206-12216 (2006).

22. Goldschen-Ohm, M. P. et al. Structure and dynamics underlying elementary ligand binding events in human pacemaking channels. *eLife.* **5**, e20797 (2016).
23. Miyake, T. et al. Real-Time Imaging of Single-Molecule Fluorescence with a Zero-Mode Waveguide for the Analysis of Protein−Protein Interaction. *Analytical Chemistry.* **80** (15), 6018-6022 (2008).
24. Zhao, J., Branagan, S. P., Bohn, P. W. Single-Molecule Enzyme Dynamics of Monomeric Sarcosine Oxidase in a Gold-Based Zero-Mode Waveguide. *Applied Spectroscopy.* **66** (2), 163-169 (2012).
25. Fore, S., Yuen, Y., Hesselink, L., Huser, T. Pulsed-interleaved excitation FRET measurements on single duplex DNA molecules inside C-shaped nanoapertures. *Nano Letters.* **7** (6), 1749-1756 (2007).
26. Rigneault, H. et al. Enhancement of single-molecule fluorescence detection in subwavelength apertures. *Physical Review Letters.* **95** (11), 117401 (2005).
27. Foquet, M. et al. Improved fabrication of zero-mode waveguides for single-molecule detection. *Journal of Applied Physics.* **103** (3), 034301 (2008).
28. Wada, J. et al. Fabrication of Zero-Mode Waveguide by Ultraviolet Nanoimprint Lithography Lift-Off Process. *Japanese Journal of Applied Physics.* **50** (6), 06GK07 (2011).
29. Fischer, U. C., Zingsheim, H. P. Submicroscopic pattern replication with visible light. *Journal of Vacuum Science and Technology.* **19** (4), 881-885 (1981).
30. Deckman, H. W., Dunsmuir, J. H. Natural lithography. *Applied Physics Letters.* **41** (4), 377-379 (1982).
31. Li, B., Zhou, D., Han, Y. Assembly and phase transitions of colloidal crystals. *Nature Reviews Materials.* **1** (2), 15011 (2016).
32. Bohn, J. J., Tikhonov, A., Asher, S. A. Colloidal crystal growth monitored by Bragg diffraction interference fringes. *Journal of Colloid and Interface Science.* **350** (2), 381-386 (2010).
33. Dimitrov, A. S., Nagayama, K. Continuous Convective Assembling of Fine Particles into Two-Dimensional Arrays on Solid Surfaces. *Langmuir.* **12** (5), 1303-1311 (1996).
34. Pisco, M. et al. Nanosphere lithography for optical fiber tip nanoprobes. *Light: Science & Applications.* **6** (5), e16229-e16229 (2017).
35. Chandramohan, A. et al. Model for large-area monolayer coverage of polystyrene nanospheres by spin coating. *Scientific Reports.* **7**, 40888 (2017).
36. Besra, L., Liu, M. A review on fundamentals and applications of electrophoretic deposition (EPD). *Progress in Materials Science.* **52** (1), 1-61 (2007).
37. Yu, J. et al. Preparation of High-Quality Colloidal Mask for Nanosphere Lithography by a Combination of Air/Water Interface Self-Assembly and Solvent Vapor Annealing. *Langmuir.* **28** (34), 12681-12689 (2012).
38. Jamiolkowski, R. M. et al. Nanoaperture fabrication via colloidal lithography for single molecule fluorescence analysis. *PLoS ONE.* **14** (10), e0222964 (2019).
39. Innocenzi, P. et al. Evaporation of Ethanol and Ethanol−Water Mixtures Studied by Time-Resolved Infrared Spectroscopy. *The Journal of Physical Chemistry A.* **112** (29), 6512-6516 (2008).
40. Rieger, J. The glass transition temperature of polystyrene. *Journal of Thermal Analysis.* **46** (3), 965-972 (1996).
41. Donev, A., Torquato, S., Stillinger, F. H., Connelly, R. Jamming in hard sphere and disk packings. *Journal of Applied Physics.* **95** (3), 989-999 (2004).

699 42. Kinz-Thompson, C. D. et al. Robustly Passivated, Gold Nanoaperture Arrays for Single-
700 Molecule Fluorescence Microscopy. *ACS Nano.* **7** (9), 8158-8166 (2013).
701 43. Korlach, J. et al. Selective aluminum passivation for targeted immobilization of single DNA
702 polymerase molecules in zero-mode waveguide nanostructures. *Proceedings of the National*
703 *Academy of Sciences of the United States of America.* **105** (4), 1176-1181 (2008).
704 44. Chandradoss, S. D. et al. Surface passivation for single-molecule protein studies. *Journal of*
705 *Visualized Experiments.* (86), e50549 (2014).
706 45. Plénat, T., Yoshizawa, S., Fourmy, D. DNA-Guided Delivery of Single Molecules into Zero-Mode
707 Waveguides. *ACS Applied Materials & Interfaces.* **9** (36), 30561-30566 (2017).
708 46. Kudalkar, E. M., Davis, T. N., Asbury, C. L. Single-Molecule Total Internal Reflection
709 Fluorescence Microscopy. *Cold Spring Harbor protocols.* **2016** (5), pdb.top077800 (2016).
710 47. Schindelin, J. et al. Fiji: an open-source platform for biological-image analysis. *Nature*
711 *Methods.* **9** (7), 676-682 (2012).
712 48. Hoogenboom, J. P., Derks, D., Vergeer, P., Blaaderen, A. v. Stacking faults in colloidal crystals
713 grown by sedimentation. *The Journal of Chemical Physics.* **117** (24), 11320-11328 (2002).
714 49. Micheletto, R., Fukuda, H., Ohtsu, M. A Simple Method for the Production of a Two-
715 Dimensional, Ordered Array of Small Latex Particles. *Langmuir.* **11** (9), 3333-3336 (1995).
716 50. Denkov, N. et al. Mechanism of formation of two-dimensional crystals from latex particles on
717 substrates. *Langmuir.* **8** (12), 3183-3190 (1992).
718 51. Okubo, T. Convectional, sedimentation and drying dissipative patterns of colloidal crystals of
719 poly(methyl methacrylate) spheres on a watch glass. *Colloid and Polymer Science.* **286** (11), 1307-
720 1315 (2008).
721 52. Ye, S., Routzahn, A. L., Carroll, R. L. Fabrication of 3D Metal Dot Arrays by Geometrically
722 Structured Dynamic Shadowing Lithography. *Langmuir.* **27** (22), 13806-13812 (2011).
723 53. Zhao, Y. et al. Dark-Field Illumination on Zero-Mode Waveguide/Microfluidic Hybrid Chip
724 Reveals T4 Replisomal Protein Interactions. *Nano Letters.* **14** (4), 1952-1960 (2014).
725 54. Goldschen-Ohm, M. P., White, D. S., Klenchin, V. A., Chanda, B., Goldsmith, R. H. Observing
726 Single-Molecule Dynamics at Millimolar Concentrations. *Angewandte Chemie International*
727 *Edition.* **56** (9), 2399-2402 (2017).
728 55. Noriega, T. R., Chen, J., Walter, P., Puglisi, J. D. Real-time observation of signal recognition
729 particle binding to actively translating ribosomes. *eLife.* **3**, e04418 (2014).
730 56. Uemura, S. et al. Real-time tRNA transit on single translating ribosomes at codon resolution.
731 *Nature.* **464** (7291), 1012-1017 (2010).
732 57. Choi, J., Puglisi, J. D. Three tRNAs on the ribosome slow translation elongation. *Proceedings*
733 *of the National Academy of Sciences of the United States of America.* **114** (52), 13691-13696
734 (2017).
735 58. Eid, J. et al. Real-Time DNA Sequencing from Single Polymerase Molecules. *Science.* **323**
736 (5910), 133-138 (2009).
737 59. Martin, W. E., Srijanto, B. R., Collier, C. P., Vosch, T., Richards, C. I. A Comparison of Single-
738 Molecule Emission in Aluminum and Gold Zero-Mode Waveguides. *The Journal of Physical*
739 *Chemistry A.* **120** (34), 6719-6727 (2016).
740 60. Wenger, J. et al. Single molecule fluorescence in rectangular nano-apertures. *Optics Express.*
741 **13** (18), 7035-7044 (2005).
742 61. Pineda, A. C., Ronis, D. Fluorescence quenching in molecules near rough metal surfaces. *The*

743 *Journal of Chemical Physics.* **83** (10), 5330-5337 (1985).
744

Figure 1

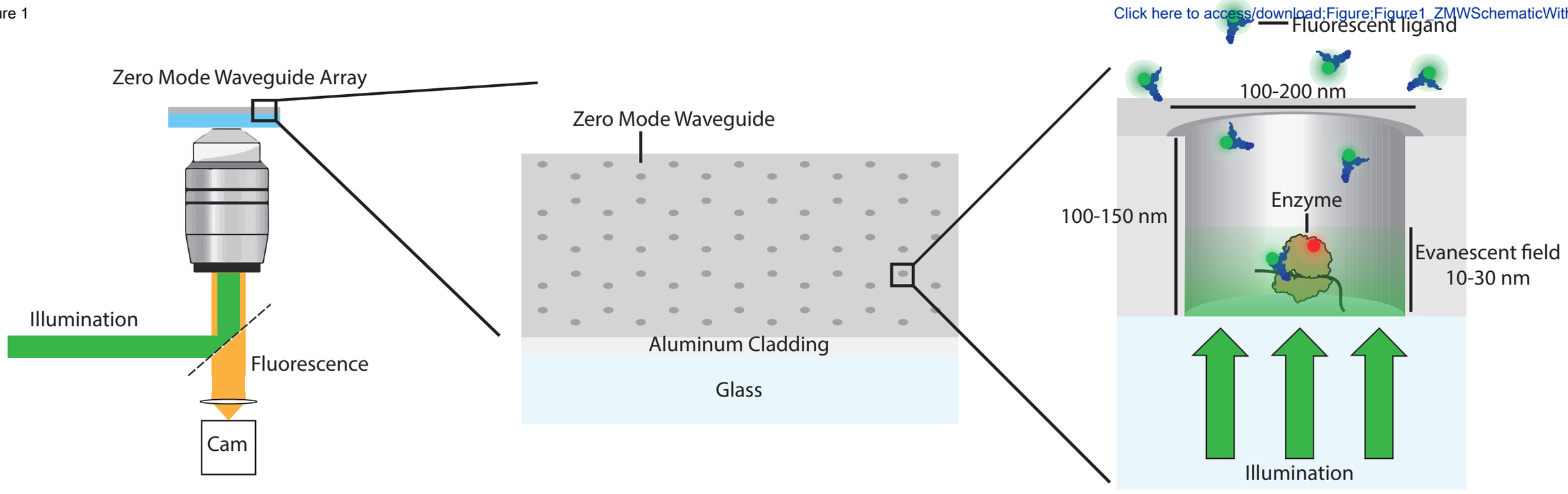

Figure 2

Click here to access/download;Figure;Figure2_AluminumFabricationSche

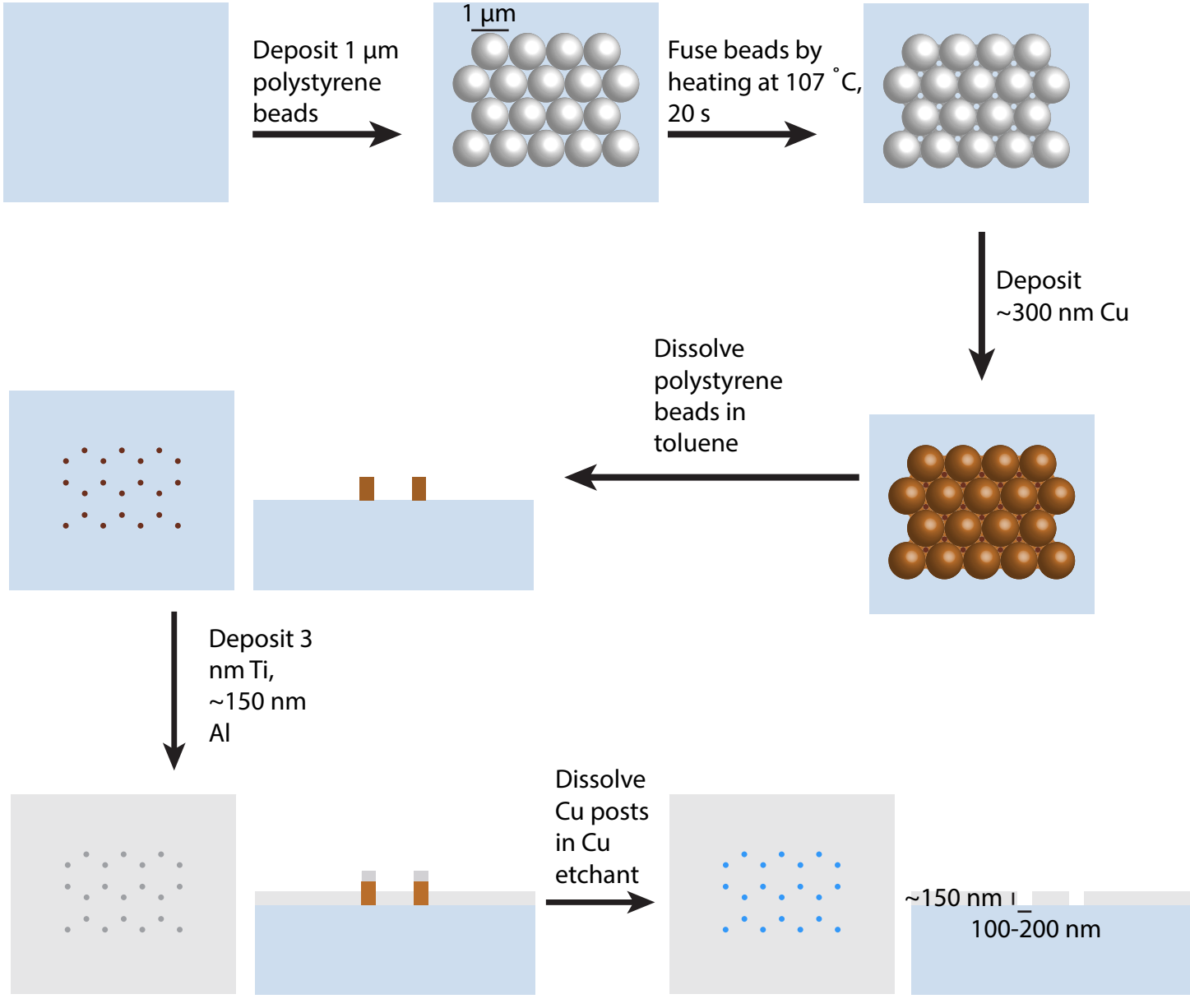

Figure 3

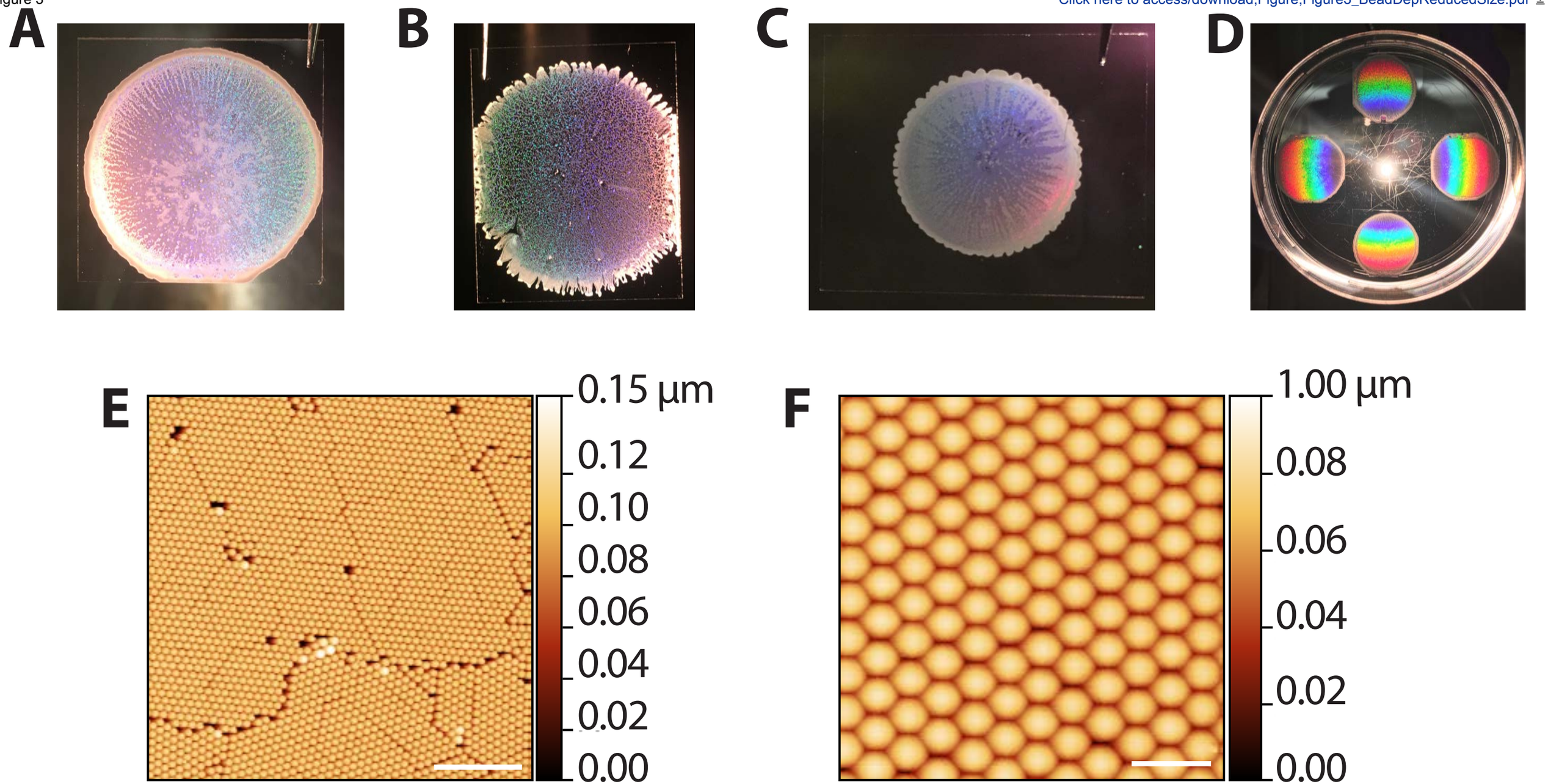

Figure 4

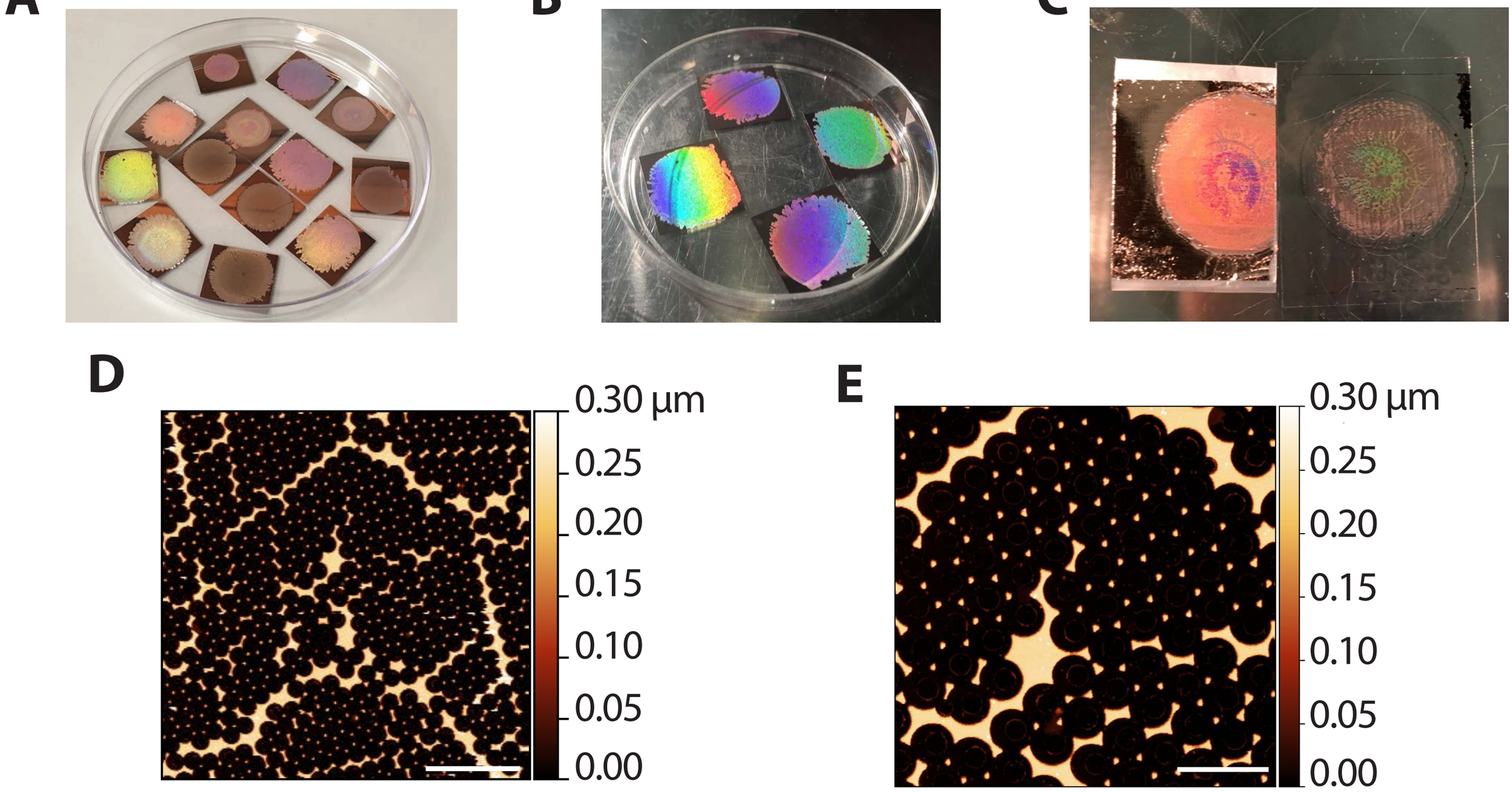

Figure 5

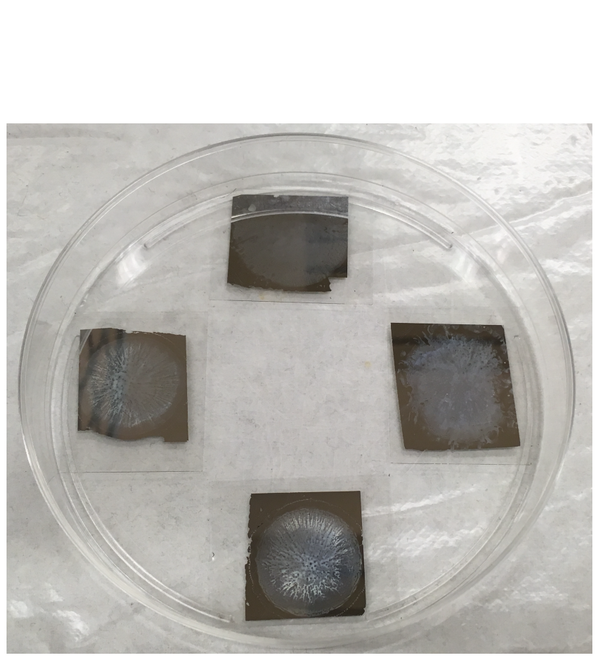

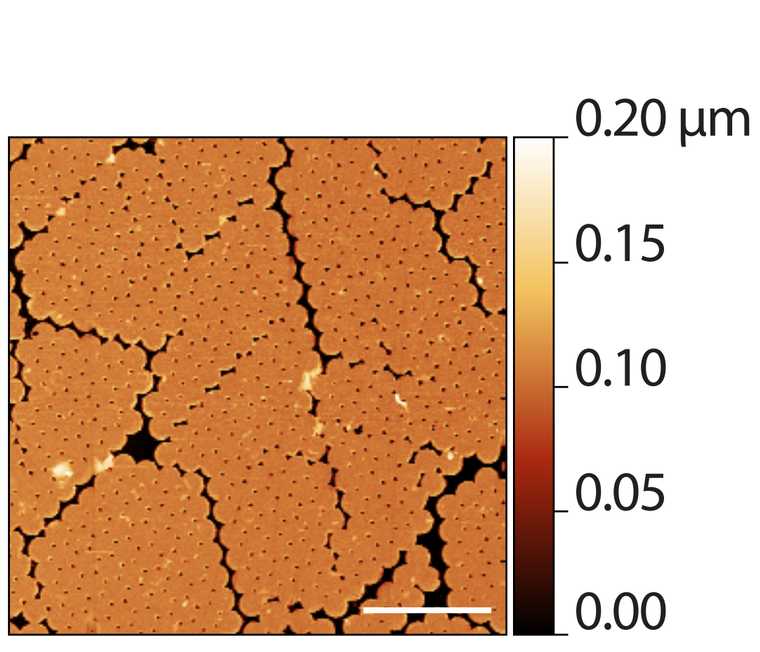

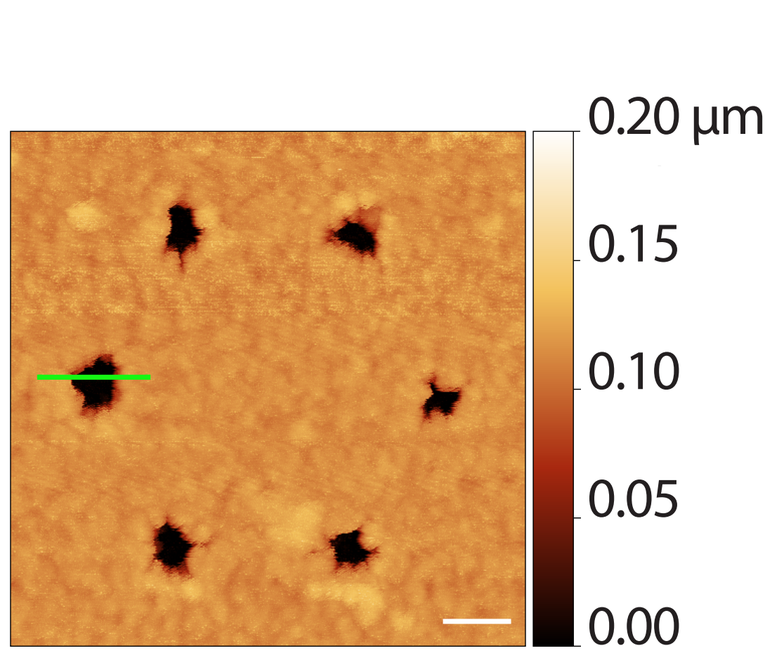

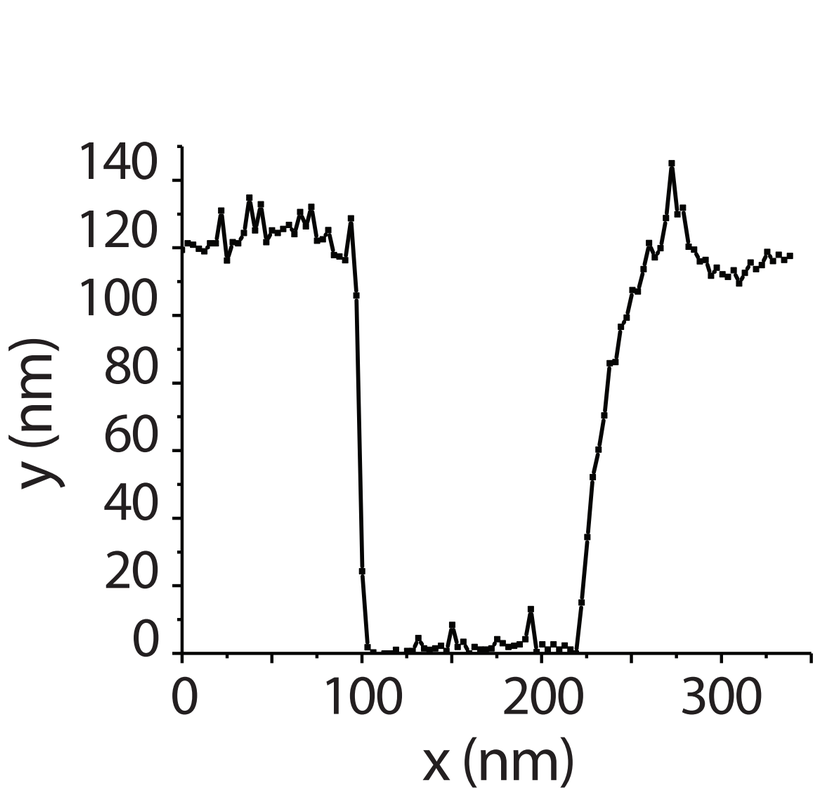

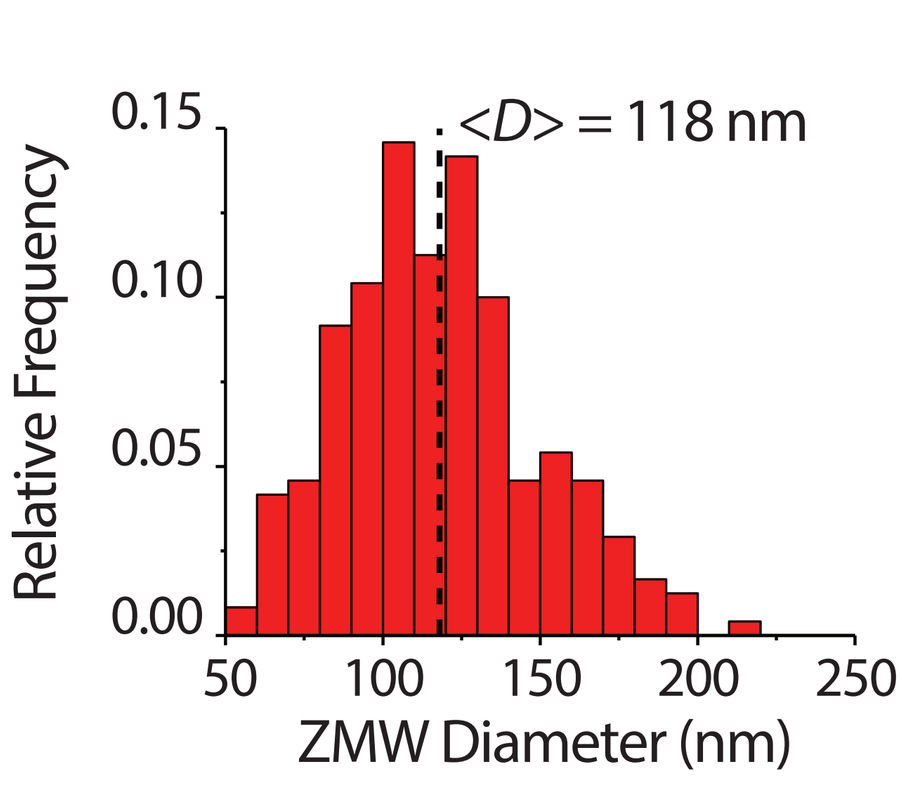

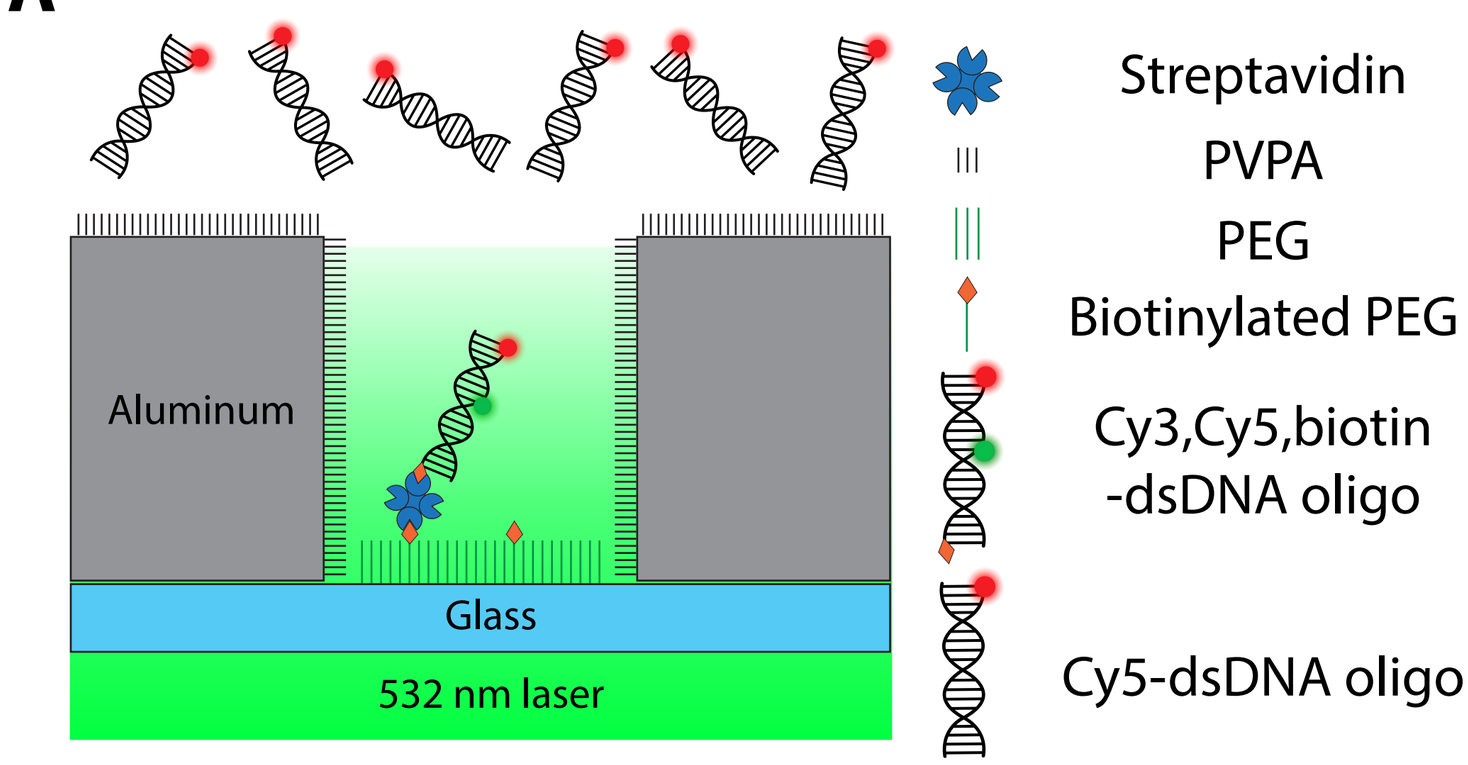

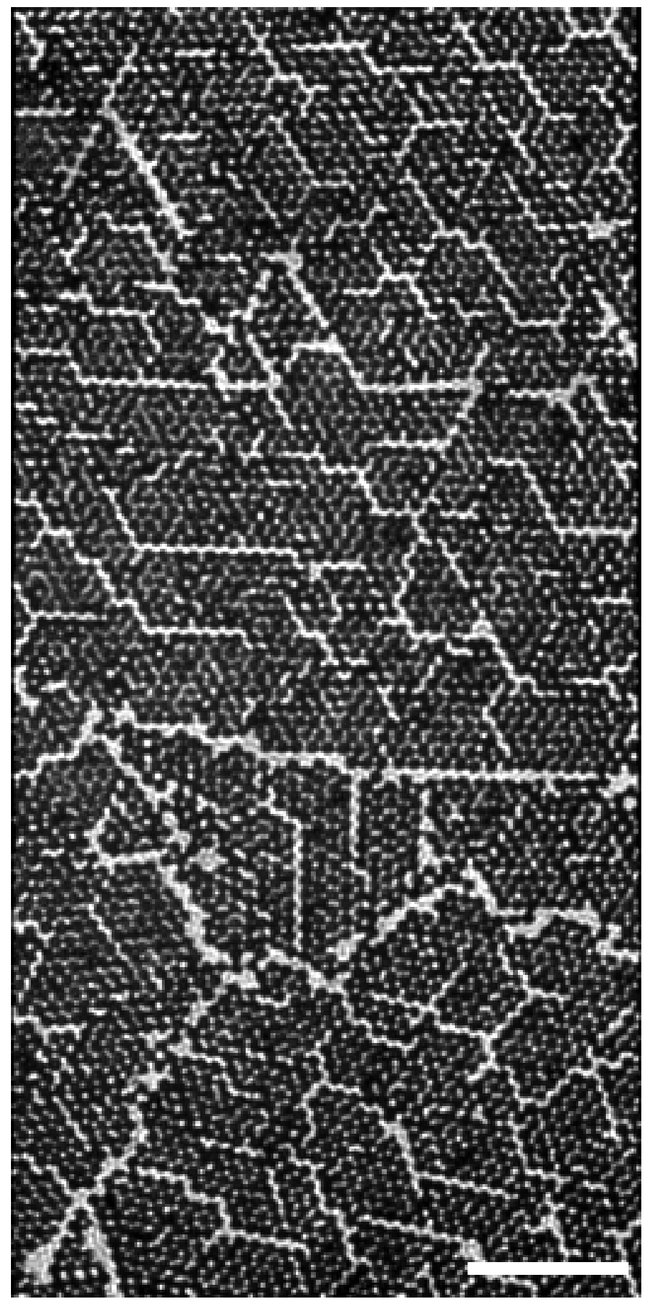

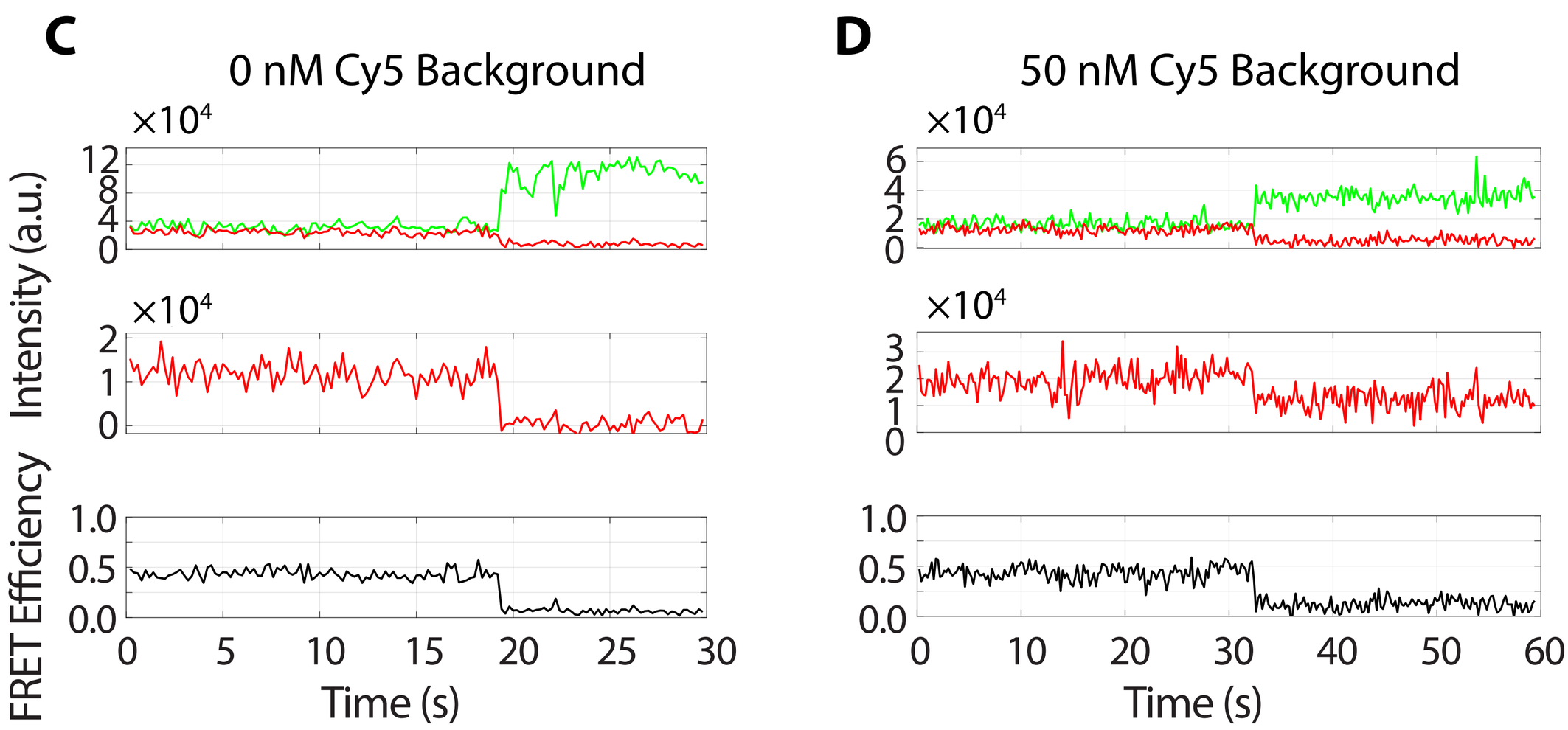

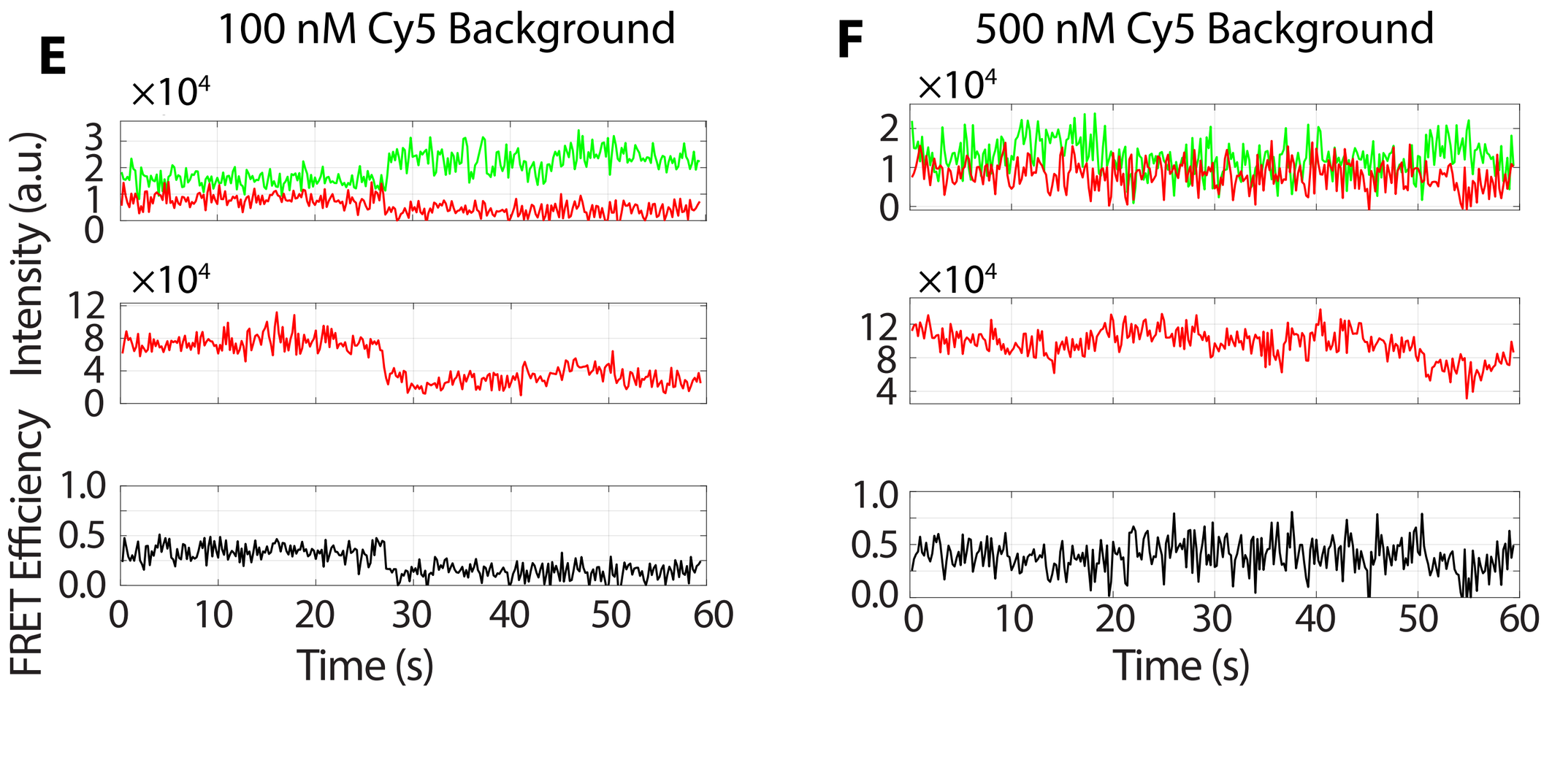

Table of Materials

Click here to access/download;Table of Materials;61154_Materials_Submission_07_02_20_revise.xls

Name of Material/Equipment	Company	Catalog Number	Comments/Description
1. Glass Coverslip Cleaning			
Acetone	Sigma	32201	1 L
Coplin glass staining jar	Fisher Scientific	08-817	Staining jar with 8 grooves and molded glass cover
Coverslips	VWR	48404-467	24 mm x 30 mm (No.1½, Rectangular)
Ethanol	Sigma	E7023	1 L
KOH	Sigma	30603	Potassium hydroxide
Petri dishes	Fisher Scientific	R80115TS	100 mm diameter, 15 mm deep
Sonicator	Branson	Z245143	Tabletop ultrasonic cleaner, 5510
2. Evaporative Deposition of Polystyrene Beads			
Clear storage container	Fisher Scientific	50-110-8222	26 x 18 x 15 in.
Desk fan	O2Cool	FD05001A	Any small desk (~5 in.) fan will work
Glass beaker	Fisher Scientific	02-555-25B	250 mL
Humidity meter	Fisher Scientific	11-661-19	
Microcentrifuge tubes	Fisher Scientific	21-402-903	1.5 mL
Polystyrene microspheres	Polysciences	18602-15	1.00 µm diameter, non-functionalized
Triton X-100 deturgent	Sigma	X100	100 mL
3. Bead Annealing for Reducing Pore Size in the Colloidal Crystal Template			
Aluminum plate	Fisher Scientific	AA11062RY	Customized in-house to 14 cm x 14 cm
Ceramic hotplate	Fisher Scientific	HP88857100	13 x 8.2 x 3.8 in.
Temperature controller	McMaster-Carr	38615K71	Read temperature with thermocouple probe

Thermocouple probe	McMaster-Carr	9251T93	Type K, surface probe
4/5. Nanofabrication of Zero Mode Waveguides Using the Colloidal Crystal Template			
Aluminum etchant	Transene	Type A	
Aluminum pellets	Kurt J. Lesker	EVMAL40QXHB	For electron beam evaporation
Chloroform	Sigma	288306	1 L
Copper etchant	Transene	49-1	
Copper pellets	Kurt J. Lesker	EVMCU40QXQA	For electron beam evaporation
Gold pellets	Kurt J. Lesker	EVMAUXX40G	For electron beam evaporation
Lens paper	Thorlabs	MC-5	
Plasma cleaner	Harrick Plasma	PDC-32G	
Scotch tape	Staples	MMM119	
Thin film deposition system	Kurt J. Lesker	PVD-75	Tabletop thermal evaporation system will also work
Titanium pellets	Kurt J. Lesker	EVMTI45QXQA	For electron beam evaporation
Toluene	Sigma	244511	1 L
Representative Results			
COMSOL Multiphysics Modeling So	COMSOL, Inc.		
Dual View spectral splitter	Photometrics, Inc.		

We are grateful for the great care and expertise that the referees have shared and for their supportive comments. Many of the suggestions from the referees are very reasonable comparisons to other ZMWs and ways to adjust the fabrication protocol. Most of these were already included in our PLOS One paper on this subject[1]. Because the purpose of this JOVE submission is to provide more detail and instruction on fabrication method, we did not repeat all of those comparisons here. We do refer more clearly, as mentioned below, to those points that were published before. Changes in the manuscript noted below appear in red in the resubmitted version.

Editorial comments:

Changes to be made by the author(s):

1. Please take this opportunity to thoroughly proofread the manuscript to ensure that there are no spelling or grammar issues. The JoVE editor will not copy-edit your manuscript and any errors in the submitted revision may be present in the published version.

We have read through the manuscript to check for spelling and grammar issues.

2. Please revise lines 41-43 and 100-101 to avoid textual overlap with previously published work.

We have revised the text in those lines to avoid textual overlap.

3. Please revise the Protocol to contain only action items that direct the reader to do something (e.g., "Do this," "Ensure that," etc.). The actions should be described in the imperative tense in complete sentences wherever possible. Avoid usage of phrases such as "could be," "should be," and "would be" throughout the Protocol. Any text that cannot be written in the imperative tense may be added as a "NOTE."

We have revised the protocol to only include steps with action items.

4. Please number the figures in the sequence in which you refer to them in the manuscript text.

We have read through the manuscript and ensured that all figures are referred to in sequence. Figure S2 and S3 have been switched to correct this.

5. Figure 2: Please change the time unit "sec" to "s" (i.e., 20 s).

We have changed the time unit from "sec" to "s" in the figures.

6. Table of Materials: Please sort the materials alphabetically by material name.

We have sorted the materials alphabetically within in each section of the materials list.

Reviewers' comments:
Reviewer #1:
Manuscript Summary:
In the presented work K. Chen and co-authors illustrate how nanostructures such as ZMWs can be obtained by colloidal, or nanosphere,
lithography. This is an alternative strategy, with respect to others more expensive and time consuming, to create nanometer-scale masks for waveguide
fabrication. The report describes the approach in detail, with practical considerations for each phase. The method allows thousands of aluminum or gold ZMWs to be made in parallel, with final waveguide diameters and depths of 100-150 nm.

In my opinion the report is well written and very clear to the reader.
I recommend the publication

We thank the reviewer for these comments.

Reviewer #2:
Manuscript Summary:
This manuscript describes a protocol for fabrication of zero mode waveguides (ZMWs) based on colloidal or nanosphere lithography as an alternative to commonly used electron beam lithography or ion beam milling. Fabrication of ZMWs using colloidal or nanosphere lithography is simple and inexpensive. The authors also illustrate an application of the ZMWs for single molecule imaging at higher concentrations.

Minor Concerns:

1. Although fabrication of ZMWs by using the proposed protocol in this manuscript is simple and less expensive, there appears to be a wide distribution of ZMW size. They show 100-150 nm in the figures and in the text in some place and others 100-200 nm. It is not clear if they mean that this encompasses the heterogeneity of hole sizes in a typical preparation. Or is this the range of holes that can be made. The distribution in figure 5e shows a somewhat wider distribution.

We thank the reviewer for catching this inconsistency. There is some variability both within each sample and among samples. 100-200 nm captures most of the distribution of ZMW diameters in Figure 5e, and we have made this consistent in all the figures and text. This range performs well in single molecule fluorescence experiments.

2. Can the ZMW diameter be varied? It would be great to mention directions to make ZMWs with lower or higher than 100 nm in diameter.

We thank the reviewer for this insightful comment. The ZMW diameters can indeed be varied by tuning the melting time in Part 3 of the Protocol. In a previous publication[1], we

characterized the pore size in the waveguide template as melting time was varied (Figure 2e-h in Jamiolkowski et al., 2019). The data show that the pore diameter can be made larger by reducing the melting time, but cannot be made much smaller than 100 nm since pores begin to quickly close past 20-25 sec of annealing. Assuming that users of the method will want the smallest possible pore diameter for maximal fluorescence background reduction, we used the 20 sec melting time in the detailed JoVE protocol. We now refer more clearly in the Discussion to the earlier paper in regard to varying pore size.

3. Line 215 says "3. Bead Annealing for Tuning the Size and Shape of the Colloidal Crystal Template" But there is no information in this section about how to tune the size or shape.

We agree that this section does not provide data on how the pore size varies with melting time. We intend for this JoVE article to provide more details on how to practically implement the method we described in a previous paper[1], so we omit the pore size versus annealing time data. However, we changed the title of the section to “Bead Annealing for Reducing Pore Size in the Colloidal Crystal Template” so that it will not be misleading. We refer to the earlier paper in the Discussion in regard to varying pore size.

4. Line 191 provide the rational for keeping the chamber temperature warmer than room temperature

Rather than a parameter we controlled, the temperature in the chamber was an effect of the hot water evaporation in the closed system. However, the ambient chamber temperature affects the temperature of the ethanol-bead suspension, which can affect the ethanol evaporation rate. The evaporation rate determines how well the beads pack, so we mentioned the temperature we typically see in the chamber when we perform the protocol. However, since the temperature is not explicitly controlled, typically only 1-2 °C higher than room temperature, and not a critical parameter, we de-emphasized the importance of controlling the temperature (lines 213-215).

5. In the fabrication section, the final rinse is with DI water. Even with EBL a final descum etching with subsequent acid wash is necessary to clean up ZMWs. Does rinsing with DI water remove any fluorescent traces? This would be surprising.

We thank the reviewer for this comment. We agree that non-specific fluorescence from insufficiently cleaned slides is a concern for single molecule microscopy, and indeed we do sometimes see nonspecific fluorescent particles during TIRF imaging. We typically bleach these particles with the excitation laser before loading sample into the ZMWs. We are aware that previous papers fabricating ZMWs with electron beam lithography (EBL) use a photoresist stripper[2] or oxygen plasma[3,4] to remove residual resist, but since we are not using electron resist, we did not need to use either cleaning method

after dissolution of the copper posts. However, we did include an oxygen plasma cleaning step after dissolution of the polystyrene template to remove any residual polystyrene (step 4a.4). A previous study using EBL to fabricate gold ZMWs[5] also did not use a descum etching or acid wash step after fabrication and used a simple water and isopropyl alcohol wash after functionalization of the ZMWs with polyethylene glycol (PEG). Based on these considerations, the protocol as described worked well.

6. Line 275 provide the composition of copper and aluminum etchant

We would like to provide the full composition of the copper and aluminum etchant, but the manufacturer of both etchants (Transene) unfortunately does not provide this on their website. However, based on information from a "Copper Etchant 49-1 White Paper" on the Transene website (https://transene.com/wp-content/uploads/Copper-Etch-Article.pdf) and an aluminum etchant type A MSDS from Sigma Aldrich (Product Number 901539), we know the copper etchant is citric acid-based and the aluminum etchant type A (standard aluminum etchant for silicon devices) is phosphoric acid-based. We have indicated this in the Protocol (lines 304-305 and 339-340).

7. Line 572 Typo double "into the"

We thank the reviewer for catching this typo and have fixed it in the manuscript.

Reviewer #3:
Manuscript Summary:
Interesting technique. Generally well described.

Major Concerns:
1. Would be helpful to have a schematic with excitation source and detector (camera?) to show how these SMWs are actually used.

We thank the reviewer for this suggestion and have added an excitation source, objective, and detector to the schematic in Figure 1.

2. Is it possible to have a diagram showing how they compare to the more conventional ones?
In our previous publication[1], we compared the single molecule fluorescence signal to noise ratio from our ZMWs to those of gold ZMWs from another publication[5] using electron beam lithography. Because we wanted to focus on the practical details of implementing the protocol in this article, we did not include this data. We now refer to the earlier paper for this comparison in the Discussion.

3. Do any of the steps produce residues that impact the background?

Yes, the bead annealing step (part 3 of Protocol) increases the likelihood of the polystyrene beads leaving a residue on the glass slide prior to the second metal deposition, which can interfere with metal adherence to the glass. However, we mention in the Discussion that the overnight toluene soak resolves the issue.

4. What is the average number of SMWs that are simultaneously analyzed? How does this impact the statistical signiicance of the results?

Figure 6b shows a typical field of ZMWs in a dual-view TIRF setup with 100x magnification. More than 3000 waveguides are contained in that image. Assuming a conservative estimate of 10% loading based on Poisson statistics, one can obtain a statistically significant sample size of several hundred single molecule traces from a few movies of different spots on the ZMW slide. This was done in Figure 5 of our previous publication[1] introducing the method.

Minor Concerns:
p.2 and 3, not clear to what "their" refers. Avoid use of ambiguous pronouns.

We thank the reviewer for catching this and have removed ambiguous uses of the “their” pronoun in the manuscript.

p.5 Specify time that coverslips can be stored prior to that the last sentenceach step or use.

We thank the reviewer for suggesting this addition. We have added notes for where the protocol can be stopped and how to best the store the templates and ZMW slides for later use.

p.7 Needs to be more clear in the protocol which steps are for gold ZMWs. After reading this section, it was not clear whether the copper deposition step also applies for the gold AMWs and whether the aluminum is also deposited over the copper for the aluminum ZMWs.

We have now separated the aluminum and gold ZMW protocols into two separate subsections (part 4a and 4b of Protocol).

p.7. It would probably help to describe what "excess" looks like since the metal posts need to stay in place.

We have added more description to the note after the tape pull (lines 272-277).

p. 8. Add caution about proper storage of Chloroform.

We thank the reviewer for catching this omission and have added notes about storage for chloroform, toluene, and the metal etchants.

p.13. Not clear what the " channels" are or what their relationship is to the ZMWs.

We have clarified in the manuscript that the channels are individual ~20 μL flow chambers[6] that can be used for successive single molecule experiments on the same ZMW slide.

Reviewer #4:
Manuscript Summary:
This paper is a simple fabrication method paper, which focuses on fabricating ZMW surface without accessing to specialized nanofabrication facilities. The method described here is simply written. This paper will contribute to widely expand single molecule measurements using ZMW to the lab or research institution including even small group scale. This paper should be published.

We thank the reviewer for these comments.

Reviewer #5:
Manuscript Summary:
The manuscript describes a relatively cheap and ascetic way of fabricating zero-mode waveguides (ZMW), which provide drastic improvement to signal-to-background and signal-to-noise ratios of single-molecule FRET(sm-FRET) experiments. The authors employ nanosphere lithography to achieve down to 100 nm diameter ZMW which are benchmarked using a basic sm-FRET experiment. The distinct feature of the method is using minimal amount of expensive equipment to fabricate sub-diffraction limit ZMW and make the technology available to broader scope of scientists.

Major Concerns:
1. Since the method described is meant for low-resource (in terms of fabrication facility) setting and is in a sense a novel approach for fabrication of ZMW, I feel that the manuscript lacks a concrete and critical discussion on the limitations of such a fabrication method (i.e. resolution, reproducibility, distribution of ZMW sizes and factors affecting it). Looking at the figures it feels like authors have sufficient data to characterize their method better and pin-point some critical parameters and how they affect the quality.

We thank the reviewer for this comment and agree that, as a new method, data should be provided on the distribution of ZMW sizes and reproducibility of ZMW sizes. For this JoVE article, we focus on the practical implementation of the method, and data on the limitations has already been provided in a previous publication[1] introducing the method. Fig. S4 of that paper describes the batch-to-batch variation in ZMW diameters, which is mostly due to differences in melting time during the annealing step (part 3 of the

Protocol). The limit on the resolution of our fabrication method is also due to pores closing in the bead template once the pores reach a threshold size (discussed in lines 558-565). The variation in ZMW sizes within a representative individual slide is provided in Fig. 5E and is comparable to the variation of ZMW sizes within an individual slide fabricated with electron beam lithography in a previous paper using gold ZMWs (Fig. 2 of Kinz-Thompson et al., 2013[5]). Overall, duplicating the characterization published before would be redundant, but we cite that work more clearly now.

2. The proposed protocol contains a very peculiar way of creating controlled humidity environment, through placing a fan above a glass of hot water in a plastic box. Though humidity has been demonstrated by the authors to be a critical parameter affecting the quality of colloidal crystal, reproducing of this particular conditions for achieving right humidity looks tricky. Retrieving or manipulating samples in such setting requires going into the box and disrupting the inside conditions, which makes the method quite operator dependent. Obviously the method has proven to be viable, but it is necessary to describe a way of adapting this protocol to using it in glove box (setting up a humidity glove box can be actually not a very expensive/complicated task) for more reproducible humidity conditions.

We thank the reviewer for this suggestion and would like to mention that we did consider using a humidity-controlled glove box to improve control of the deposition conditions. However, we did not have ready access to a humidity-controlled glove box in our lab and found that it was simple enough and effective to adjust the starting humidity in the plastic chamber on the bench by waiting longer or shorter times for the humidity to rise. We agree with the reviewer that the humidity changes as we go into the box each time to deposit the beads. We acknowledge this in the Results and recommend users only perform 6 depositions at a time. However, even with beads deposited towards the end when the humidity has dropped by about 10%, there is still 1-2 cm^2 of useable bead monolayer area (Fig. 1C) for ZMW templating. Lastly, each deposition takes 10-15 min, so users can quickly improve the depositions by adjusting the starting humidity with each iteration. We do not feel it is necessary to repeat the experiments with a glove box in order to state that as an alternative. We do now mention that a similar atmosphere could also be achieved in a glove box (lines 213-215).

3. The method itself is based on a double lift-off using first the polystyrene mask and then a metal mask generated after first metal evaporation. I was missing a discussion on metal selection for these processes (particularly copper , which is quite a nasty metal and makes this protocol harder to implement in a clean environment) In principle Cr mask should also be possible to use and to be etched away orthogonally to aluminium in Cr etchant. Also on the second lift-off step the authors rather used metal thickness compared to the mask thickness with ratio 2:1 (150 nm metal to 200-300nm pillars) This thickness ratio is borderlining to not resolve the liftoff (usual rule for lift-off is mask: metal 3:1) I would like to ask authors to comment about the metal thickness limitations and whether they experienced any liftoff problems at certain ratios.

4. Figure 1 and Figure 2 contain '3D' projections of the sample, but they are shown without perspective and hence hey look misleading instead of helping to understand the process. Images should either be converted to 2D or perspective should be introduced

We thank the reviewer for these comments. We did originally consider using chromium to create the first metal mask, but chromium etchant, unfortunately, also etches aluminum (https://transene.com/etch-compatibility/). We also tried using gold for the first metal mask, but gold etchant also etched away aluminum. Another gold etchant composed of zinc cyanide and potassium cyanide is indicated as compatible with aluminum on the Transene website, but we avoided the use of cyanide-based etchant due to its toxicity. Besides copper etchant, Ti-Tungsten etchant is another etchant compatible with aluminum, but this would etch the titanium layer used for aluminum adhesion to glass. Lastly, copper etchant is relatively safe to use and is mostly composed of citric acid. Thus, the choices of materials and etchants had a rational basis, and they worked well in our hands.

The reviewer is also correct in pointing out that the aluminum metal cladding thickness did pose some problems for metal post dissolution, which is why we introduced the rubbing step to access the posts for dissolution (steps 4a.7 or 4b.7). We have included a note (lines 300-302) to caution users about the thickness of the aluminum cladding. We also mentioned in the Discussion that the posts are likely pyramidal in shape, which increases the likelihood of the aluminum cladding covering the sides of the posts during deposition. We suggest in the Discussion that users can increase copper height for easier copper post dissolution and should ensure that sample plate holders are not rotating during aluminum deposition. However, we found that with the rub step, dissolution of almost all the copper posts (Fig. 5B) was consistently achievable with 1:3 – 1:2 ratios of aluminum cladding:copper post height (100 nm:300 nm – 150 nm:300 nm).

We also thank the reviewer for pointing out the lack of perspective in Figures 1 and 2 and have changed the cross-sectional views to 2D to reduce confusion.

Minor Concerns:
1) I think that readability of the paper can be dramatically improved if the authors could a) remove redundancy between results and discussions (or reshuffle the text to eliminate the redundancy of certain paragraphs)
b) provide careful linking between protocol-results - discussion. Everywhere in the protocol where the point is expanded to results or discussion - state it. And vice versus - everything that is discussed in results and discussion has to have reference to the particular points of the protocol that are discussed.

We thank the reviewer for this suggestion. We have taken care to read through the manuscript and remove or reshuffle redundant text in the Protocol, Results, and Discussion. We have also added references to the Results and Discussion in the

Protocol and references to the Protocol steps in the Results and Discussion. We believe this has improved readability of the manuscript.

c) Some of the figures contain panels that are not mentioned in text, text mentions Figure 7, where there is no Figure 7. Some of the figures carry the S prefix, where there is no distinct supplementary material attached

We thank the reviewer for catching these errors. For the supplementary figures, JoVE does not have separate sections for supplementary material, but does allow supplementary figures, which are labeled with the S prefix. These figures were included in the submission, and we have referenced all of them in the Results and Discussion.

Though this is a minor concern, I think it should be taken seriously by the authors
2) Authors suggest cleaning of the slide from the polysterine beads after first metal deposition using toluene overnight. Did the authors consider somewhat more harsh , but more efficient removals like RCA1 (could work for copper and Cr, but not for Aluminium). More efficient cleaning between the liftoff steps could provide better resolution and reproducibility

We thank the reviewer for this helpful suggestion and have added this in the Discussion as a possible modification to step 4a.4/4b.4 (lines 593-595).

3) The authors have mentioned dependence of the ZMW size on annealing time. It looks like they have sufficient imaging data to plot some calibration curve like diameter of ZMW vs annealing time. It would be very helpful for people who try to reproduce the protocol.

We thank the reviewer for this suggestion. We have done this in a previous publication introducing the method[1] (Figure 2 of Jamiolkowski et al., 2019). We focus on the practical implementation of the method in this JoVE article and refer to the earlier publication for this data.

4)The authors offer using the protocol for making both gold and aluminium ZMW, but the parts of the protocol that describe it are written out in a confusing manner since for gold ZMW pillars should be made out of aluminium. Therefore I suggest to split the gold ZMW in a separate small subprotocol.

We have separated the aluminum and gold ZMW protocols into two separate subsections (part 4a and 4b of Protocol).

5) It would be also worth mentioning nanoimprint lithography as a method for fabrication of ZMWs.

We thank the reviewer for bringing this method to our attention and have added it to the Introduction (lines 98-103).

Reviewer #6:

Manuscript Summary:

The authors describe a protocol for a unique and convenient fabrication of zero-mode wave guides via nanosphere lithography which circumvents the expense and time associated with traditional e-beam lithography or FIB approaches. While the fabrication protocol is detailed, the manuscript is lacking in details on how to test the fabricated ZMWs in a single-molecule experiment as no protocol was provided for testing ZMWs post fabrication. Further, it is unclear why devices fabricated via this approach have a dramatically lower maximal concentration (~200 times lower than expected) compared to devices fabricated by standard approaches. Given the understandable desire to make ZMWs more accessible to the broader biochemistry community with a less expensive fabrication scheme, it is important to add a discussion about the limitations of ZMWs fabricated via this approach. In revised form that addresses the comments below, this manuscript would be acceptable for publication.

Page Line Comment

- 1 39 The focus on single-molecule enzymology in the abstract and manuscript is a bit narrow and ignores the many labs that are using ZMWs to study other systems. The focus instead should be on studying weak-affinity interactions (e.g. enzyme-substrates, protein-ligand interactions, protein-protein interactions). The authors may consider reviewing and citing the following comprehensive and up-to-date review of ZMWs:

Crouch, Garrison & Han, Donghoon & Bohn, Paul. (2018). Zero-mode waveguide nanophotonic structures for single molecule characterization. Journal of Physics D: Applied Physics. 51. 193001. 10.1088/1361-6463/aab8be

We thank the reviewer for bringing this review article to our attention and have added this reference and discussion of other applications of ZMW technology to the Introduction (lines 90-93).

- 2 166 Does the fabrication of ZMWs via nanosphere lithography need to be accomplished inside a clean-room or can all steps be performed in general lab space? This should be made clear in the steps of protocol. Clean-room access itself can be limiting for production of ZMWs.

We thank the reviewer for this question. None of the steps need to be completed in a clean room. Some institutions may already have electron beam or thermal evaporation systems installed in clean rooms, but this protocol does not assume access to a clean room. We have added a note indicating this in the Protocol (line 134).

- 8 366 Details about how the authors performed the single-molecule FRET experiments

for testing ZMWs need to be included. For example, which buffers were used; what excitation source(s) were used; what was the frame rate of collection; which lasers, objectives, and detector were used? These details are necessary for the reproducibility of the experiments and validation of successful fabrication.

We thank the reviewer for catching this omission. We have added more details on the imaging protocol to the Results section (lines 397-422) as well as reference to the similar smFRET imaging protocol we used in our previous paper[1] introducing the fabrication method.

- 8 376 The fact that signal-to-noise deteriorating at 500 nM with the use of FRET inside ZMWs is concerning. FRET increases the effective concentration limit of ZMW and, in fact, Goldschen-Ohm et al., has shown that FRET in ZMWs works ups to 1 mM. The authors need to comment on why the signal-to-noise is much lower in ZMWs fabricated via nanosphere lithography compared to traditional approaches (e.g. e-beam lithography, FIB) that can get access to single digit uM.

M. P. Goldschen-Ohm, D. S. White, V. A. Klenchin, B. Chanda, R. H. Goldsmith, Angew. Chem. Int. Ed. 2017, 56, 2399.

8 378 What is the highest concentration of a freely diffusing dye (no-FRET) that the authors can still detect inside the ZMWs? Typical ZMWs have a detection limit around 1-10 μM.

We thank the reviewer for bringing this article to our attention. In our previous publication[1] introducing our method, we included single molecule data on freely diffusing dye at 0 nM, 1 nM, 10 nM, 50 nM, 500 nM, and 1 μM concentrations, consistent with the 1-10 μM detection limit that was observed for freely diffusing dye in Goldschen-Ohm et al., 2017. This detection limit was also consistent with gold ZMW data from Kinz-Thompson et al., 2013[5], who fabricated the ZMWs with electron beam lithography.

We acknowledge that the signal to noise of the acceptor dye from FRET excitation is not as high as that observed in Goldschen-Ohm et al., 2017. This could be due to differences in experimental setup. Goldschen-Ohm et al., 2016[7] suggested that the FRET efficiency between the fluorescent cyclic nucleotide and DyLight650 on the cyclic nucleotide binding domain was near 100%, while the apparent FRET efficiency between our oligo bound Cy3 and Cy5 was around 50%. In addition, the donor dye rather than the acceptor dye was freely diffusing in solution in Goldschen-Ohm et al. In contrast, our experiment had the acceptor dye diffusing in solution. Since Goldschen-Ohm et al. varied the concentration of the donor dye, the acceptor dye trace from FRET was likely less affected by higher concentrations. Another previous study (Zhao et al., 2014)[8] measuring FRET in EBL-fabricated ZMWs also reported issues with nonspecific binding of the diffusing acceptor labeled protein to the ZMWs, making FRET difficult to resolve at diffusing acceptor concentrations higher than 1 μM. We have added discussion on

the FRET concentration limit to the text (lines 598-612).

9 431 In Figure 6 (or elsewhere), could the authors provide the average spacing between ZMWs?

We thank the reviewer for catching this omission. The distance between the centers of adjacent ZMWs is set by the hexagonal close packing of the 1 μm beads ($\frac{2}{\sqrt{3}} * 500\ nm = 557\ nm$). The average waveguide spacing of 559 nm measured in the high-resolution AFM image in Figure 5C is consistent with the packing geometry. We have added this to the Results (lines 389-392).

11 492 Thorough cleaning of the cover-glasses prior to ZMW fabrication is indeed critical for successful metal deposition. However, the proposed method herein uses a crude cleaning procedure (KOH, organic washes) compared to the more commonly used cleaning methods, such as SC-1, piranha, or oxygen plasma. Could the authors comment on how this cleaning protocol was established and why more robust procedures were not used?

We thank the reviewer for this question. In a previous JoVE article detailing a cleaning protocol for TIRF smFRET experiments[6], the glass slides were cleaned with organic washes and piranha and then used directly for imaging. We based the cleaning procedure in part 1 of the Protocol on the organic wash steps in Chandradoss et al. and found that sonication with KOH and organic solvents sufficiently cleaned the glass coverslip surfaces to obtain well-spread monolayer bead templates during part 2 of the Protocol. Since the glass slides still go through many subsequent treatments for ZMW fabrication after bead deposition, we saved additional cleaning for later steps, including plasma oxygen cleaning in step 4a.4/4b.4. We have also added in the manuscript that additional cleaning of the ZMW with aluminum compatible acid wash or Piranha can be used before passivation (lines 595-597).

References

1 Jamiolkowski, R. M. *et al.* Nanoaperture fabrication via colloidal lithography for single molecule fluorescence analysis. *PLOS ONE.* **14** (10), e0222964, (2019).

2 Foquet, M. *et al.* Improved fabrication of zero-mode waveguides for single-molecule detection. *Journal of Applied Physics.* **103** (3), 034301, (2008).

3 Levene, M. J. *et al.* Zero-mode waveguides for single-molecule analysis at high concentrations. *Science.* **299** (5607), 682-686, (2003).

4 Miyake, T. *et al.* Real-Time Imaging of Single-Molecule Fluorescence with a Zero-Mode Waveguide for the Analysis of Protein–Protein Interaction. *Analytical Chemistry.* **80** (15), 6018-6022, (2008).

5 Kinz-Thompson, C. D. *et al.* Robustly Passivated, Gold Nanoaperture Arrays for Single-Molecule Fluorescence Microscopy. *ACS Nano.* **7** (9), 8158-8166, (2013).

6 Chandradoss, S. D. *et al.* Surface passivation for single-molecule protein studies. *J Vis Exp.* 10.3791/50549 (86), (2014).

7 Goldschen-Ohm, M. P. *et al.* Structure and dynamics underlying elementary ligand binding events in human pacemaking channels. *eLife.* **5** e20797, (2016).
8 Zhao, Y. *et al.* Dark-Field Illumination on Zero-Mode Waveguide/Microfluidic Hybrid Chip Reveals T4 Replisomal Protein Interactions. *Nano Letters.* **14** (4), 1952-1960, (2014).

Figure S1

Click here to access/download;Supplemental File (Figures, Permissions,

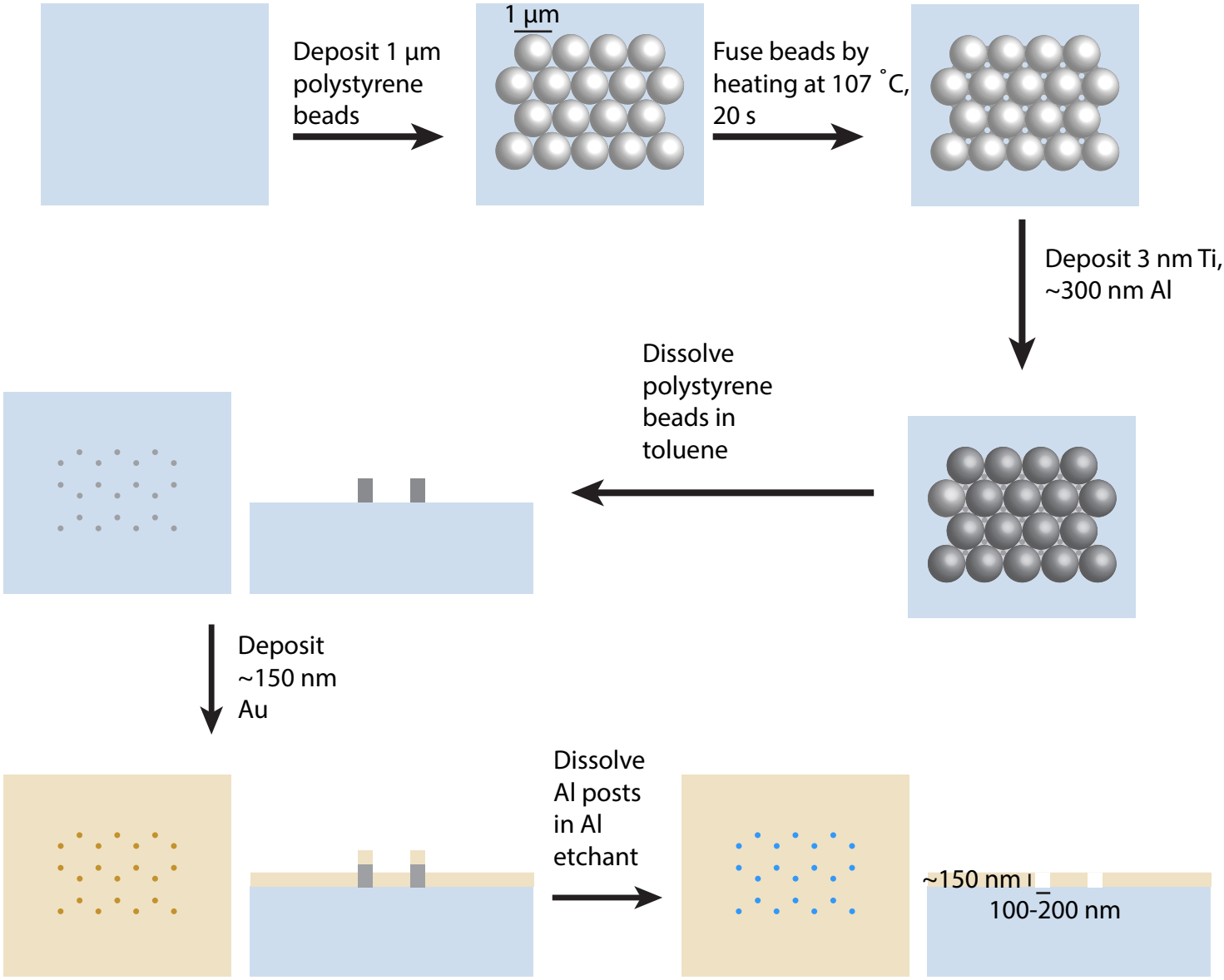

Figure S2

Click here to access/download;Supplemental File (Figures, Permissions, etc.);FigureS2_COMSOLFigure.pdf